

ROLL VIBRATION OF A RECIPROCATING
AIR COMPRESSOR

by

John H. Herold II

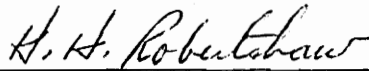
Thesis submitted to the Graduate Faculty of the
Virginia Polytechnic Institute and State University
in partial fulfillment of the requirements for the degree of

MASTER OF SCIENCE

in

Mechanical Engineering

APPROVED:



H. H. Robertshaw, Chairman



H. H. Mabie



N. S. Eiss

August, 1977

Blacksburg, Virginia

LD
5655
V855
1977
H47
c.2

ACKNOWLEDGMENTS

The author expresses sincere appreciation to the members of his advisory committee: Professors N. S. Eiss, H. H. Mabie, and H. H. Robertshaw, Chairman. The guidance and assistance of Dr. Robertshaw throughout the investigation is especially appreciated.

Appreciated also is the sponsorship of the David Taylor Naval Ship Research and Development Center of Annapolis, Maryland.

The author is indebted to a colleague, Mr. C. O. Morehead, without whose foresight, patience, and support, this study would never have become reality.

TABLE OF CONTENTS

	<u>Page</u>
TITLE	i
ACKNOWLEDGMENTS	ii
TABLE OF CONTENTS	iii
LIST OF FIGURES	v
LIST OF TABLES	vii
LIST OF SYMBOLS	viii
1 BACKGROUND	1
2 INTRODUCTION	6
3 REVIEW OF LITERATURE	9
4 APPARATUS AND TEST PROCEDURES	10
4.1 Air Compressor	10
4.2 Instrumentation	10
4.3 Data	11
4.4 Angular Accelerometer	17
5 MOTION ANALYSIS	21
5.1 Development of Governing Equation	23
5.2 Determination of Phase Angles	28
5.3 Translation of Reference Point	30
5.4 Analysis Implementation	32
6 PARAMETRIC STUDY	38
6.1 Development of Central Equations	38
6.2 Motor Model	54
6.3 Fourier Analysis	56
6.4 Program Control Logic	61
6.5 Model Verification	62
6.6 Variation Parameters.	64

TABLE OF CONTENTS (continued)

	<u>Page</u>
7 CONTROL OF ROLL VIBRATION	75
7.1 Development of Reduced-Order Equations	75
7.2 Control System Design	77
8 CONCLUSIONS	90
9 RECOMMENDATIONS	92
CITED REFERENCES	94
APPENDIX A - Simulation Code for the Motor-Compressor System: PABEWE	95
VITA	105

LIST OF FIGURES

	<u>Page</u>
1. Motor-Compressor System Schematic	4
2. Diagram of Six Modes of Vibration	7
3. Instrumentation Cart	12
4. Instrumentation Scheme	13
5. Location of Accelerometers	14
6. Example of Real Time Analyzer Output, 0-100 Hz	15
7. Example of Real Time Analyzer Output, 0-1000 Hz	16
8. Angular Accelerometer Transducer	18
9. Diagram for Motion Analysis	22
10. Schematic of Compressor Components	40
11. Geometry of the Slider-Crank Mechanism	42
12. Piston Kinematics	46
13. Free Body Diagram of Piston	48
14. Free Body Diagram of Shell	50
15. Free Body Diagram of Rotor	52
16. Test Motor Characteristic Curve	57
17. Motor Characteristic Curve as Input to PABEWE	58
18. Comparison of Measured and PABEWE Predicted Levels . .	63
19. Effect of Connecting Rod Length on the Angular Acceleration of the Shell	66
20. Effect of Crank Throw Length on the Angular Acceleration of the Shell	68

LIST OF FIGURES (continued)

	<u>Page</u>
21. Effect of Shell Moment of Inertia on the Angular Acceleration of the Shell	69
22. Effect of Rotor Moment of Inertia on the Angular Acceleration of the Shell	71
23. Effect of Piston Mass on the Angular Acceleration of the Shell	72
24. Block Diagram of Simplified Model of Roll Dynamics	76
25. Block Diagram of Simplified Model of Roll Dynamics with Disturbance Input	78
26. Block Diagram of Simplified Model of Roll Dynamics with Added Feedback	80
27. Effect of Motor Gain, K_M , on the Motor Compressor System	86
28. Effect of Varying the Controller Gain and the Feedback Gain	88

LIST OF TABLES

	<u>Page</u>
1. Motion Analysis - Development	31
2. Comparison of Measured and Standard Predicted Levels . .	34
3. Comparison of Standard and No-Roll Predicted Levels . . .	35
4. Comparison of Standard and Only-Roll Predicted Levels . .	36
5. Comparison of Standard and Only-Pitch Predicted Levels .	37
6. Motor Speed - Torque Data	55
7. Effect of Equal Piston Pressure Forces on the Angular Acceleration of the Shell	74
8. Effect of Motor Gain on Roll Vibration Levels	87

LIST OF SYMBOLS

<u>Symbol</u>	<u>Definition</u>
A	translational acceleration amplitude (m/s^2) disturbance amplitude (N-m)
a	translational acceleration (m/s^2)
C	Fourier coefficient
CG	center of gravity
CR	center of rotation
d	disturbance input (N-m)
F_c	connecting rod force (N)
F_w	cylinder wall force (N)
f_L	line frequency (Hz)
f ()	denotes functional relationship
H	angular momentum ($kg\cdot m^2/s$)
I	mass moment of inertia ($kg\cdot m^2$)
j	$\sqrt{-1}$
K	controller gain
K_M	motor gain (N-m-s/rad)
k	feedback coefficient
L	connecting rod length (mm)
M	moment (N-m)
M_p	piston mass (kg)
n	integer index

LIST OF SYMBOLS (continued)

<u>Symbol</u>	<u>Definition</u>
P	period of rotor rotation (sec)
PF	piston pressure force (N)
p	point designation
R	crank throw length (mm)
R(t)	reference signal
r	difference of accelerometer coordinates (m)
r_M	distance of piston from crank shaft (m)
s	Laplace variable (s^{-1})
SLIP	slip speed (rad/s)
T_M	motor torque (N-m)
T_{MOUNT}	mount torque (N-m)
T_P	torque from pistons (N-m)
t	time (sec)
x	axis, coordinate
y	axis, coordinate
z	axis, coordinate
\mathcal{Q}	angular acceleration amplitude (rad/s^2)
α	angular acceleration (rad/s^2)
β	difference in rotor and shell angular positions (rad)
θ_R	rotor angle (rad)

LIST OF SYMBOLS (continued)

<u>Symbol</u>	<u>Definition</u>
θ_s	shell angle (rad)
ϕ	angle of connecting rod (rad) phase angle (rad)
Ω	frequency of rotation (rad/s)

1. BACKGROUND

Reciprocation machines utilizing a slider-crank mechanism have been employed in machine design for many years. Internal combustion engines, steam engines, pumps, and air compressors are some of the machines in which this slider-crank linkage is commonly used. Although there are several advantages to this type of linkage, it is often accompanied by machine vibration.

Several problems arise from this vibration. Gauges are difficult to read, and their internal mechanisms fail prematurely. Piping systems and mounts often are overstressed and subsequently fail. When this vibration is transmitted to living areas and working areas, it is uncomfortable. In short, these vibrations are often unacceptable.

Over the years, several approaches have been developed for reducing the vibration amplitudes:

- a) The unbalanced dynamic forces (caused by accelerating inertias) have been reduced, and in some cases eliminated, by the judicious location of counterweights, pendulums, and other linkages, within the offending machine.
- b) The accelerations caused by these forces have been reduced by increasing the overall inertia of the machine.
- c) Flywheels have been incorporated in the designs.
- d) As a last resort, the offending machine is isolated on springs or some other form of resilient mount in order to reduce the vibrations transmitted to the surrounding structures.

The author had occasion to perform vibration tests on an air compressor into which much time and effort had been invested in an attempt to construct a "perfectly balanced" machine. By employing a variation of the slider-crank mechanism the designers were able to eliminate all dynamic unbalances through the use of special devices, e.g., counterrotating masses. The air compressor was driven by a three-phase electric induction motor. The motor and air compressor were rigidly mounted to a common rigid base, and the entire unit was resiliently mounted. The air compressor vibrated unacceptably. Since the cause of the vibration was inexplicable, further development of this prototype compressor was halted.

At this point it is appropriate to outline the mechanism of this residual vibration as hypothesized by the author. Only rigid body considerations will be developed. Although no real machine components are perfectly rigid, the highest observed vibration levels occur in a frequency range in which the components are effectively rigid. The highest vibration levels occur within the 0-150 Hz range, while structural resonances occur in the frequency range above 500 Hz.

The following discussion explains the hypothesized mechanism of the residual vibration observed in the compressor system. For the following qualitative analysis it is assumed that the motor and compressor separately impose torques on the rotor, and that the rotor accelerates or decelerates according to the net sum of the motor and compressor torques. This cyclic rotor acceleration and deceleration is a rigid body rotational vibration. The shell experiences similar

torque unbalances and exhibits a similar rotational vibration.

Figure 1 will prove helpful to the following discussion.

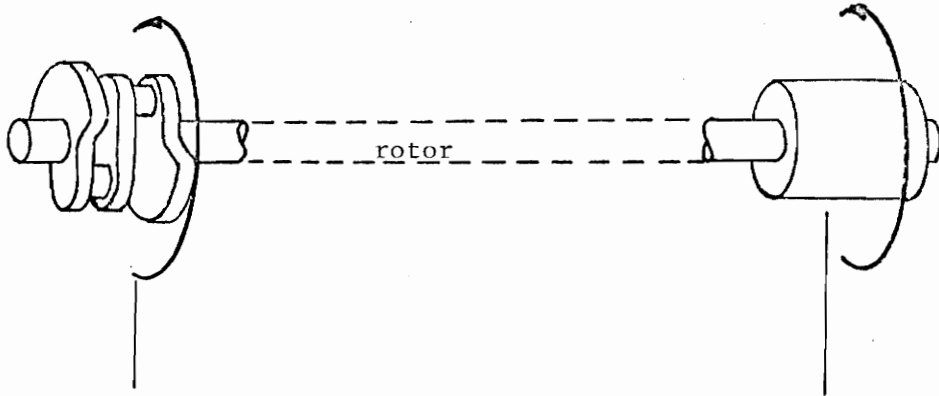
The torque imposed on the rotor by the compressor is a function of several terms. It is apparent that this torque is a strong function of the angular position of the rotor relative to the shell. The symbols θ_R and θ_S will represent the angular position of the rotor and the shell respectively, and are measured with respect to a non-accelerating reference system.

The angular speed of the rotor, and the angular speed of the rotor relative to the shell ($\dot{\theta}_R$ and $\dot{\theta}_R - \dot{\theta}_S$) also affect the torque applied by the shell to the rotor. Even the angular acceleration of the rotor and the shell ($\ddot{\theta}_R$ and $\ddot{\theta}_S$) are factors which help determine the torque applied by the shell to the rotor.

When an electric induction motor is used as a driver, the torque applied to the rotor by the motor is a function of the power supply frequency, f_L . It is also a function of the angular speed of the rotor relative to the shell, $\dot{\theta}_R - \dot{\theta}_S$.

Likewise, equations can be derived for the cyclic torque imposed on the shell by the rotor, and for determining the subsequent angular accelerations of the shell. Initially, the pistons and part of the connecting rods can be treated as part of the shell; however, they will be treated more rigorously later in this study.

The foregoing discussion and Figure 1 describe a complex dynamic relationship which could yield cyclic phenomena since there is no reason to believe f_1 will always equal f_2 .



Torque of Compressor on rotor

$$=f_1(\ddot{\theta}_r, \ddot{\theta}_s, \dot{\theta}_r, \dot{\theta}_s, \theta_r, \theta_s)$$

Torque of rotor on compressor

Torque of motor on rotor

$$=f_2(f_L, \dot{\theta}_r, \dot{\theta}_s)$$

Torque of rotor on motor

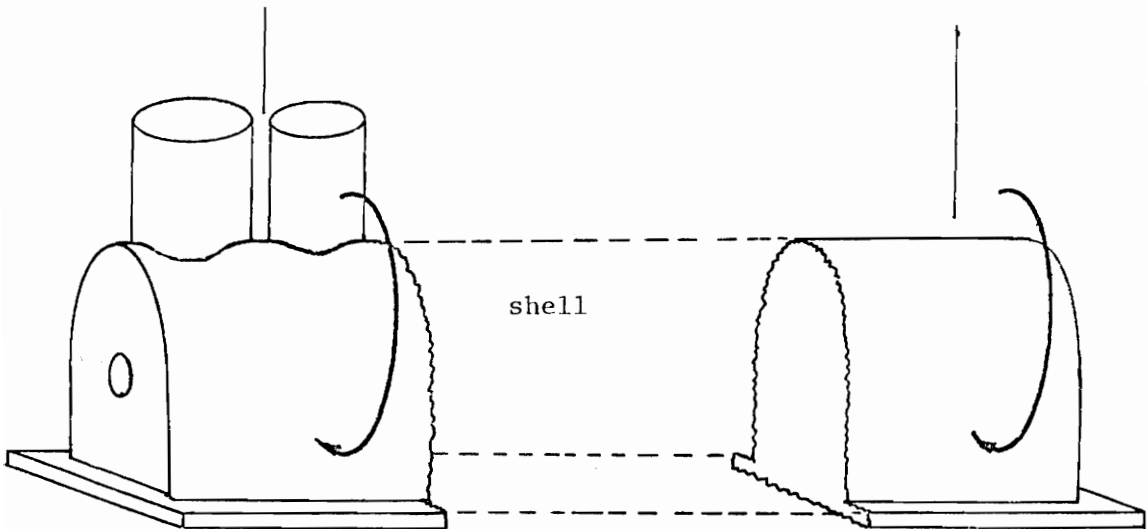


Figure 1. Motor-Compressor System Schematic

Heretofore unexplainable vibration levels have been observed in a "perfectly balanced" machine, and a mechanism of rigid-body rotational vibration has been hypothesized and qualitatively demonstrated. The financial support of the David Taylor Naval Ship Research and Development Center, DTNSRDC, was solicited and secured for further support of the investigation of this phenomenon.

2. INTRODUCTION

In the most general treatment, an air compressor vibrates in six orthogonal modes, three translational and three rotary modes. These are shown in Fig. 2. DTNSRDC was primarily interested in reducing the vibrations transmitted from the compressor to the surrounding structures via the mounts. Therefore, only those modes causing points in the x-y plane to translate in the z-direction are of interest in this study, owing to the standard technique of resilient mounting employed by DTNSRDC. The modes which contribute to this vibration are roll, pitch, and pure z-direction translation. Of these three modes, roll alone will be given in-depth treatment since the study originated as a study of roll vibration in machinery.

This study is divided into three parts:

1) Motion Analysis

The motion analysis will consist of the development of equations which describe the motion in the z-direction of points in the x-y plane. Input to these equations will be roll, pitch, and z-translation acceleration magnitudes and phases, and the x-y coordinates of the points. These equations will provide a thorough understanding of the contribution of roll to the total transmitted vibrations.

2) Parametric Study

The parametric study will examine the effects of changing various compressor design parameters, e.g., crank throw length, connecting rod length, and piston weights, on the

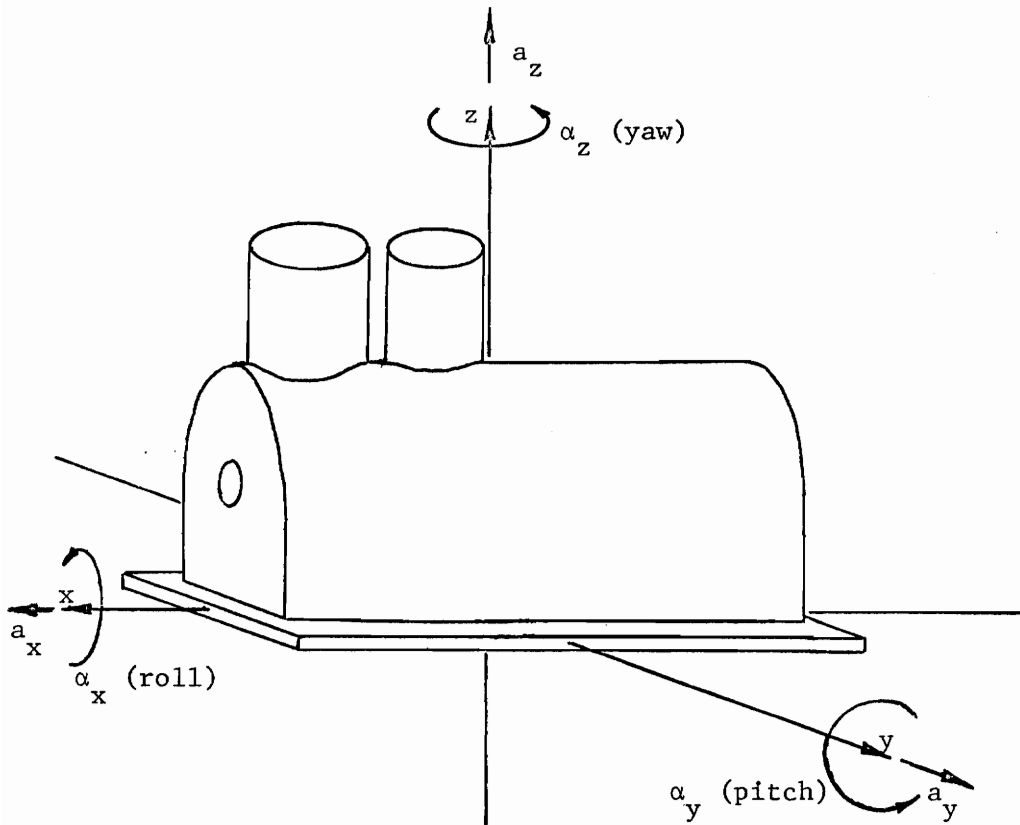


Figure 2. Diagram of Six Modes of Vibration

roll mode of vibration. This will provide designers with curves and design criteria pertinent to the minimizing of roll vibration through standard design procedures.

3) Control

The control study will analytically develop methods of reducing roll vibration through the use of control theory, e.g., feedback.

3. LITERATURE SEARCH

A literature search for previous work pertinent to this study yielded only general information concerning computer solutions of machine dynamics. The following searches were conducted: 1) a NASA Search using the keywords: compressor, reciprocation, and vibration, and covering the years 1966-76, 2) an Engineering Index search under the topic titles: compressor, reciprocation, vibration, rotor, motor, and torque, covering the years 1960-76.

Two references were found that have an indirect bearing on this work. Gatecliff (1) analytically determined the steady-state motion of a hermetic compressor using a matrix solution. However, the study did not include an extensive motion analysis of the test compressor. The experimental work only measured linear vibration displacement in one dimension. There was no attempt to measure angular accelerations. Ishii, Imaichi, Kagorku, and Imasu (2) conducted an analysis essentially parallel to that of Gatecliff. However, there was no experimental program.

4. APPARATUS AND TEST PROCEDURES

One facet of this study involved determining the contribution of roll vibration to the accelerations observed in a real compressor. This involved measuring the accelerations in the z-direction at several points on the compressor. These measurements will be used as a data base for the motion analysis, the next section of this report. In this section, Apparatus and Test Procedures, a general description of the test compressor will be given, followed by a description of the instrumentation used for data taking. Next, a discussion of the data form and characteristics will occur, and the section is terminated by a description of the angular accelerometer developed for this study.

4.1 Air Compressor

The "perfectly balanced" compressor mentioned in the Background section was unavailable for vibration testing. Instead, the air compressor provided by DTNSRDC for testing was a standard, two-cylinder, inline, reciprocating compressor driven by a three-phase induction motor with a nominal speed of 900 rpm. To provide some idea of scale, the entire unit consisting of the motor, compressor, and common baseplate, weighs about 16×10^3 N (3600 lbf). The unit was isolation mounted on four resilient mounts. Several of the components, e.g., motor, mounts, and connecting rods, will be further discussed in later sections.

4.2 Instrumentation

The vibration instrumentation, also provided by DTNSRDC, consisted of two Unholtz Dickie 25D21 accelerometers, two Piezotronics 401A11 preamplifiers, two Piezotronics 482A power supplies, an Ithaco 456M differential amplifier, Spectral Dynamics 301C real time analyzer (RTA), 302C averagers, and 13105 translator, Tektronix 602 oscilloscope, a Hewlett-Packard 7035B x-y plotter, and a General Radio 1557A shaker. Figure 3 pictures the cart which contained most of the instrumentation utilized. The instrumentation scheme is shown in Fig. 4. Accelerometer positions on the baseplate are located and numerically designated as shown in Fig. 5. This instrumentation scheme is used routinely by the sponsor with the exception of the differencing amplifier used in place of a single-input Ithaco 254A amplifier. The differencing amplifier is employed in the measurement of angular acceleration, a technique discussed in a later section.

4.3 Data

Acceleration levels were measured at several positions on the baseplate, and differential accelerations were measured for several pairs of positions. All measurements were taken at standard compressor operating conditions. Representative data are shown in Figs. 6 and 7. Typically, levels were taken from this data and tabulated rather than working with the x-y plotter output extensively. Translational accelerations are presented in zero-peak decibels (dB re: 1×10^{-5} m/s²). Rotational, i.e., angular, accelerations are presented in zero-peak decibels (dB re: 1 rad/s^2).



Figure 3. Instrumentation Cart

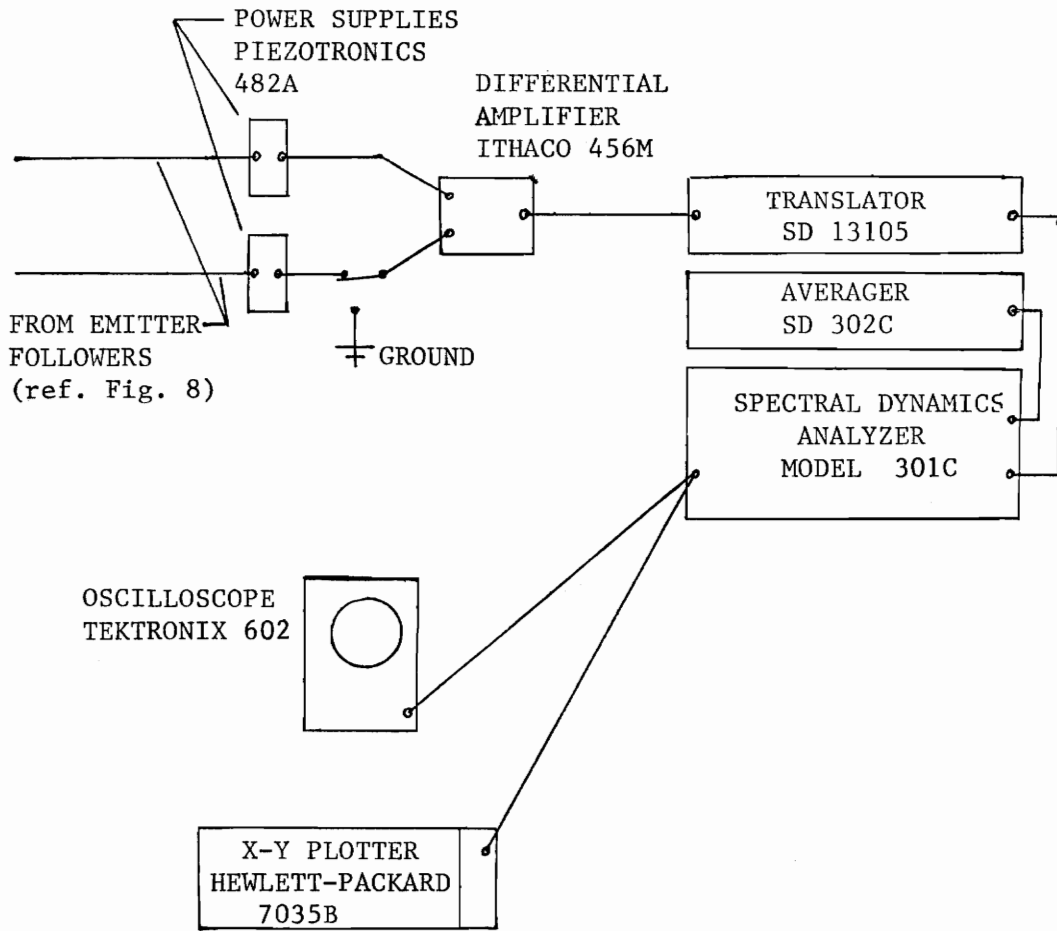
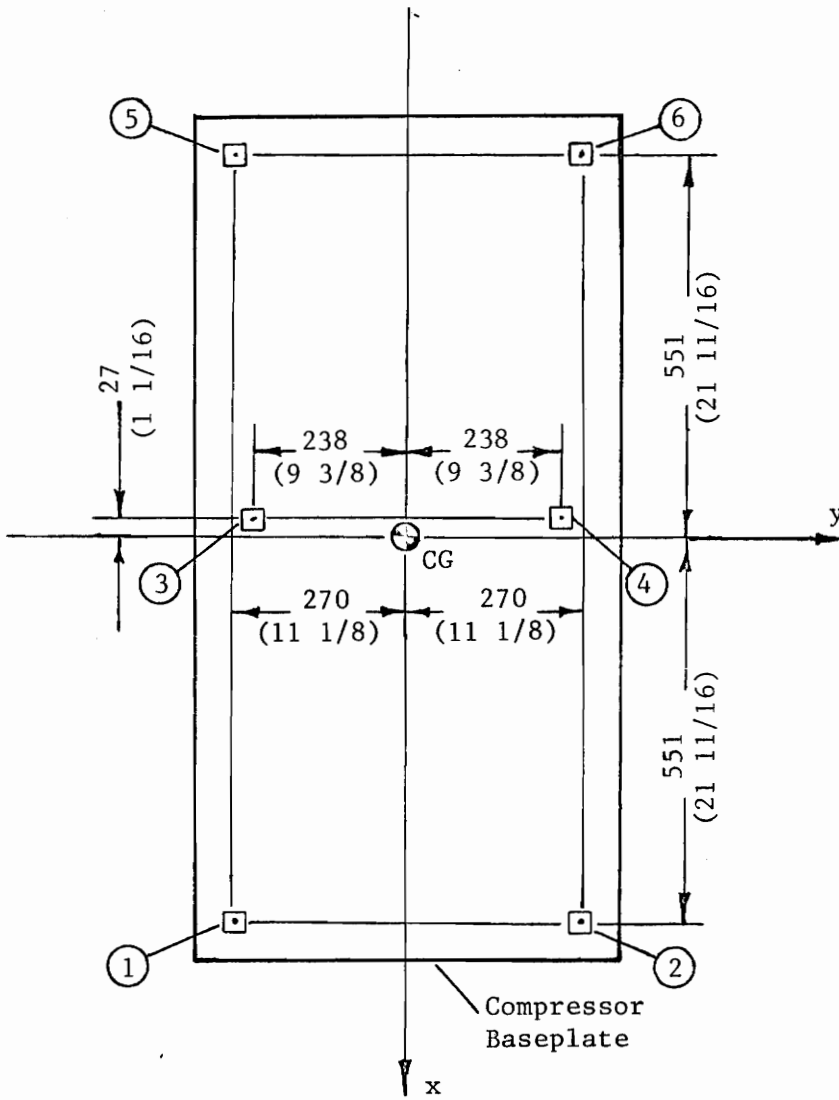


Figure 4. Instrumentation Scheme



all dimensions given in $\frac{\text{mm}}{\text{(in.)}}$.

Figure 5. Location of Accelerometers

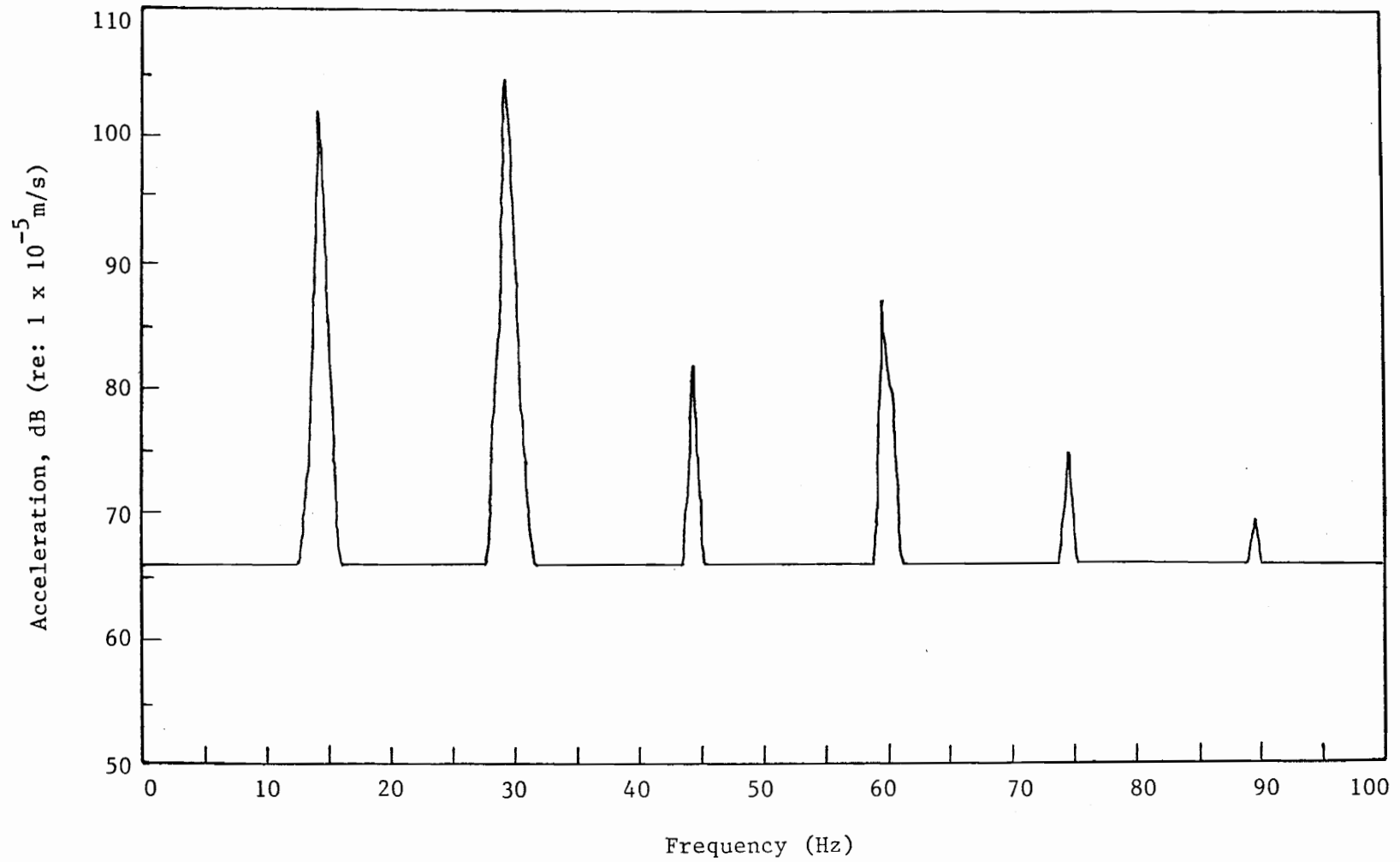


Figure 6. Example of Real Time Analyzer Output, 0-100 Hz.

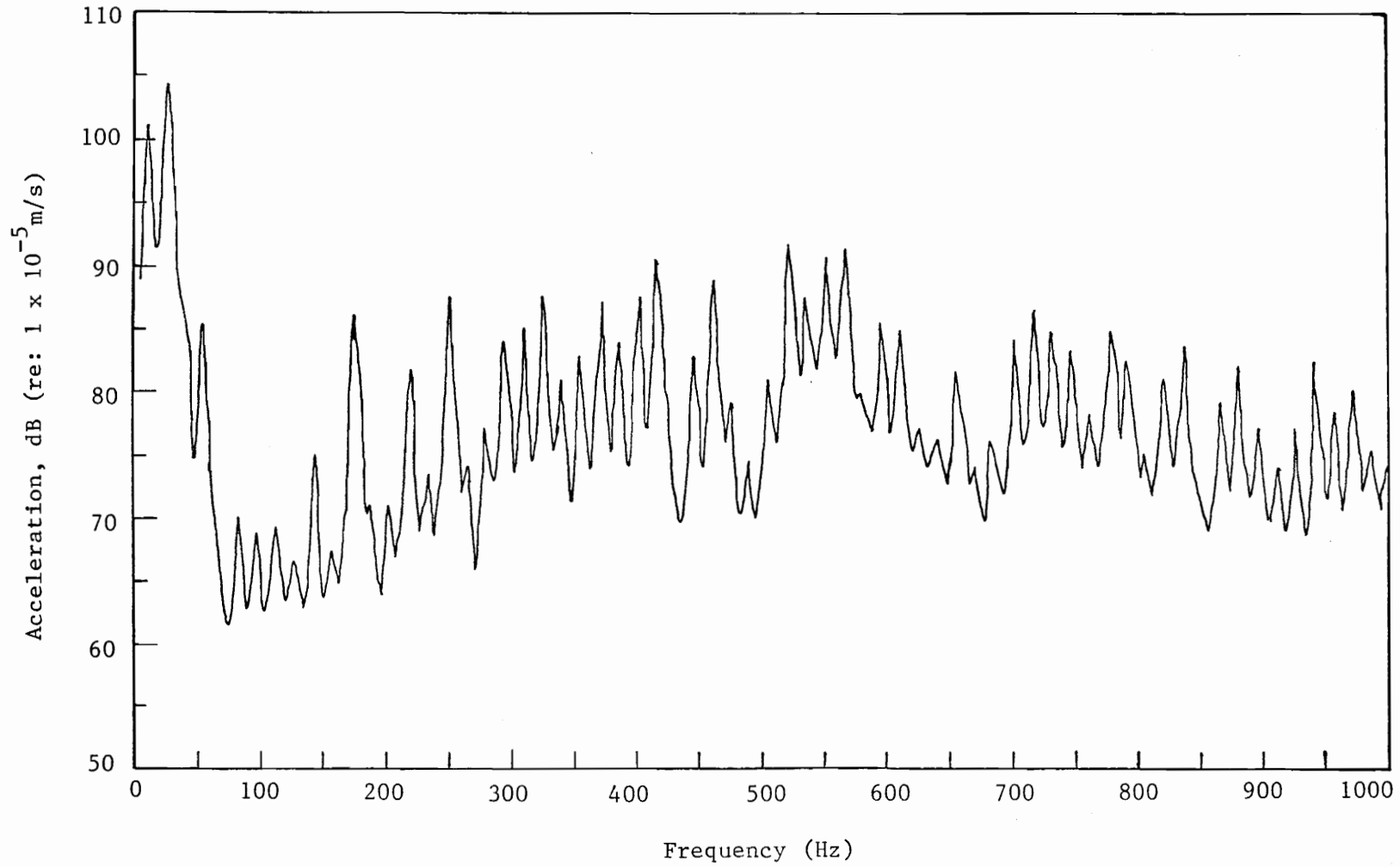


Figure 7. Example of Real Time Analyzer Output, 0-1000 Hz.

The air compressor has a fundamental exciting frequency of 15 Hz. This frequency and the next nine harmonics were considered in this study. Analyses were often limited to the first three harmonics for the following reasons: Because of the typically low levels of the eighth, ninth, and tenth harmonics, and the convenience of the 1-100 Hz window on the RTA, data presented was often limited to the first seven harmonics. The fifth, sixth, and seventh harmonics were often so much lower than the first four harmonics, that the fifth, sixth, and seventh harmonics often exceeded the dynamic range of the analyzer. The fourth harmonic, which fell just below 60 Hz, was often obscured by 60 Hz noise, particularly during the measurement of angular accelerations. Several attempts to eliminate this noise, i.e., equipment isolation, co-axial signal cable, resulted in a reduction of the 60 Hz noise, but failed to bring the noise below the level of the fourth harmonic.

4.4 Angular Accelerometer

In order to effectively study roll vibration, some method of measuring angular acceleration was required. Since commercially available angular accelerometers were inadequate for the purposes of this study, (they typically had a resonant frequency of 15 Hz) an angular accelerometer capable of measuring accelerations at much higher frequencies was required and developed. The angular accelerometer used in this study consisted of two axial accelerometers (sensitive only to accelerations parallel to one of their axes) utilized as shown in Fig. 8. The kinematic relationship between the acceleration of two

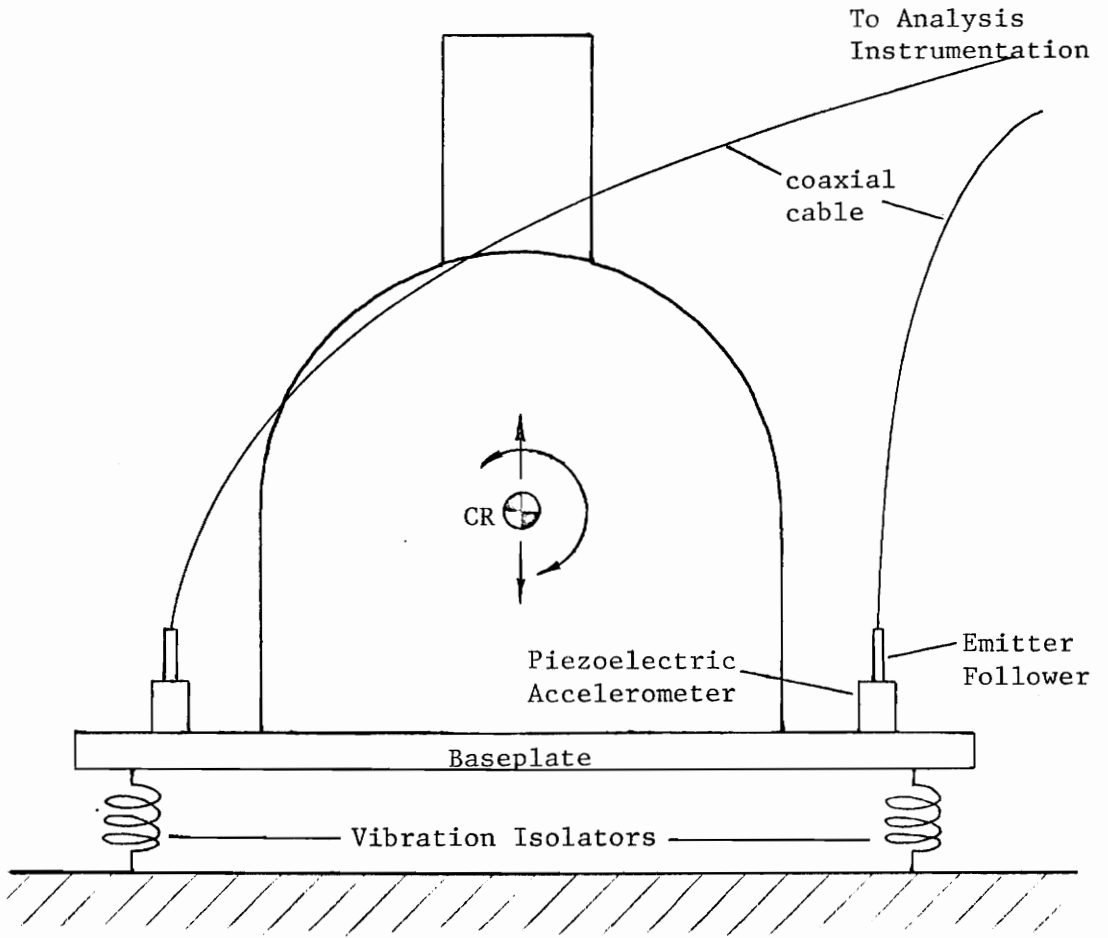


Figure 8. Angular Accelerometer Transducer

points in a rigid body is given below.

$$\vec{a}_B = \vec{a}_A + \vec{a}_{B/A} \quad (1)$$

If the body containing points A and B was accelerating in the z-direction and had no angular acceleration, the acceleration of points A and B would be identical, for a net difference of zero. Any difference in the z-direction acceleration of points A and B is due to the angular acceleration of the body. In addition, considering only acceleration in the z-direction, we have

$$a_{B/A} = r\ddot{\theta} = r\alpha, \quad (2)$$

where r is the distance from A to B and $\ddot{\theta}$ (or α) is the angular acceleration of the body. Therefore

$$\ddot{\theta} = \frac{a_{B/A}}{r} = \frac{a_B - a_A}{r}. \quad (3)$$

Provided the accelerometers are initially or artificially matched in sensitivity and phase response, the electrical output of the differencing amplifier will be proportional to $a_B - a_A$. The quantity r can be measured. Therefore, if the accelerometers have negligible cross sensitivity the response of the "angular accelerometer" is limited only by the response of the individual accelerometers, which typically have a resonance of 15 kHz. To verify the validity of the assumptions made, a test was devised. The two accelerometers were positioned 2.54 cm (1.0 in.) from each other on the compressor base,

and their outputs were inputted to the differencing amplifier. They were both receiving practically identical inputs. With the accelerometer signals differenced, all levels were at least 25 dB below the levels of single accelerometer. As a final step before taking data, the entire data acquisition system was calibrated based on accelerometer sensitivity specifications and verified with a General Radio 1557A shaker.

5. MOTION ANALYSIS

In this section the contribution of roll vibration to the acceleration levels observed in the test compressor is determined. This is done through the development of equations which characterize the motion of the compressor, and are written as a function of roll vibration amplitudes.

Given certain measured quantities, the acceleration levels in the z-direction of any point in the x-y plane (plane of the compressor baseplate) can be analytically determined. Additionally, the levels at any point in any plane parallel to the x-y plane can be determined. The accuracy of the determined levels, depending only on the accuracy of the laboratory measurements made, is typically ± 0.5 dB, i.e., ± 6 per cent. The acceleration levels for a point can be expressed as a function of roll, pitch, and pure z-direction translation, thus providing a thorough knowledge of the contribution of each mode. The development of these equations which follow was based on the assumption of small angular displacements.

The equations were developed using accelerometer positions 1, 2, and 5 as shown in Fig. 9. Certain symmetries are apparent in the x-y coordinates of accelerometer positions 1, 2, and 5. The only symmetries required by this development are

- 1) The x-coordinates of points 1 and 2 must be identical.
- 2) The y-coordinates of points 1 and 5 must be identical.

By the method of superposition, separate linear solutions for each

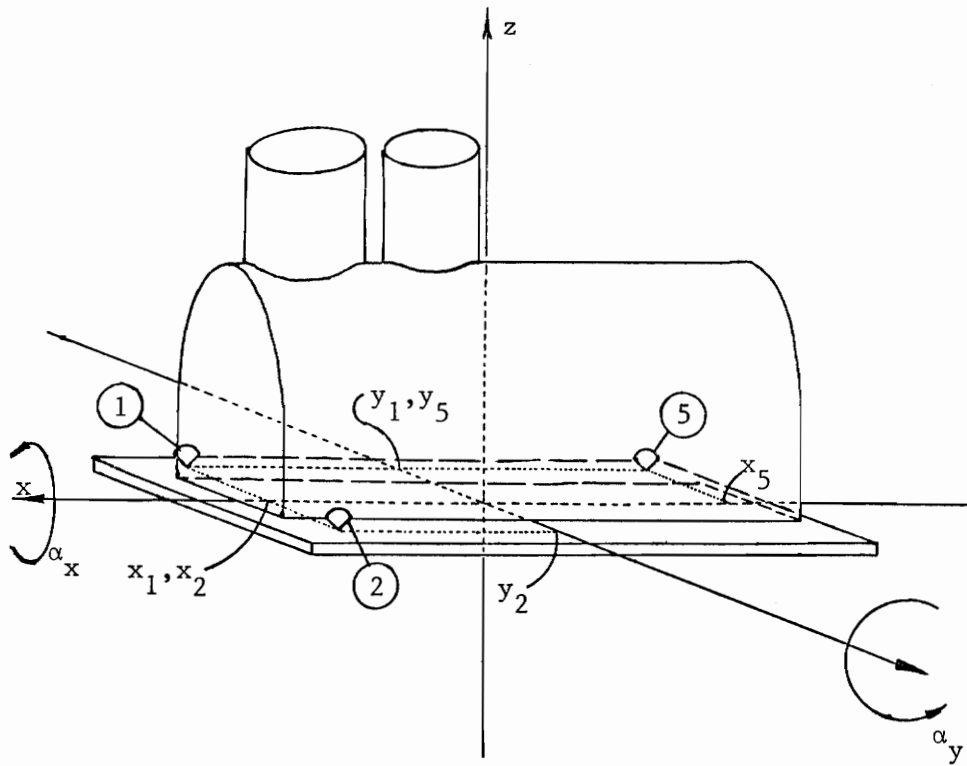


Figure 9. Diagram for Motion Analysis

orthogonal direction are added to arrive at a total solution. The remainder of this section is divided into four areas: 1) development of the governing equation, 2) determination of phase angles, 3) translation of the reference point, and 4) analysis implementation.

5.1 Development of Governing Equation

First, consider the motion in the z-direction of two points on a line parallel to the y-axis, points 1 and 2. From Eq. 1,

$$\vec{a}_2 = \vec{a}_1 + \vec{a}_{2/1}. \quad (1a)$$

The subscripts indicate position numbers, and the slash (/) is read as "relative to." Equation 3, while correct for instantaneous accelerations, is also valid for each of the Fourier components of the accelerations where a_1 , a_2 , and $a_{2/1}$ now represent time varying vectors. For a given harmonic component corresponding to a frequency, Ω , the total acceleration at position 2 can be represented by an amplitude, A_2 , and a phase angle relative to the total acceleration at position 1, $\phi_{2/1}$.

$$\vec{a}_2 = A_2 e^{j(\Omega t + \phi_{2/1})}. \quad (4)$$

Similarly, for position 1, since position 1 is the reference position,

$$\vec{a}_1 = A_1 e^{j\Omega t}. \quad (5)$$

The discussion of $a_{2/1}$ is more complex, and demands digression. From vector analysis of motion (3), at any given instant, the z-direction

acceleration of point 2 relative to point 1 is given as

$$\vec{a}_{2/1} = \vec{\alpha}_x \times \vec{r}_{12}. \quad (6)$$

The vector $\vec{\alpha}_x$, representing the angular acceleration about the x-axis, is parallel to (actually coincident with) the x-axis. The vector \vec{r}_{12} , representing the position vector of point 2 relative to point 1, is parallel to the y-axis, and therefore perpendicular to $\vec{\alpha}_x$. Therefore, Eq. 6 reduces to

$$a_{2/1} = \alpha_x r_{12}. \quad (7)$$

The term r_{12} is the difference in the y-coordinates of positions 1 and 2, and is represented as y_{21} , denoting the order of the differencing.

$$r_{12} = y_{21} = y_2 - y_1. \quad (8)$$

Generally, y_{21} may be either positive or negative. Similarly, α_x may be positive (during counterclockwise acceleration) or negative (during clockwise acceleration). Returning now to the discussion of harmonic motion, for the same given frequency, Ω , the harmonic angular acceleration about the x-axis is now expressed as

$$\vec{\alpha}_x = \alpha_x e^{j(\Omega t + \phi_{\alpha x/1})}, \quad (9)$$

where α_x is the amplitude of the angular acceleration, and $\phi_{\alpha x/1}$ is the phase of the angular acceleration relative to the motion at

position 1. From Eqs. 7, 8, and 9,

$$a_{2/1} = \alpha_x r_{12} = y_{21} \alpha_x e^{j(\Omega t + \phi_{\alpha x/1})}. \quad (10)$$

Equation 10 indicates that $a_{2/1}$ is also a vector with amplitude A_{21} such that

$$A_{21} = |y_{21}| \alpha_x. \quad (11)$$

The absolute value sign is required because while y_{21} may be either positive or negative, A_{21} , as a magnitude, must be positive. Since the absolute value sign is included in Eq. 11,

$$A_{21} = A_{12}. \quad (12)$$

The two representations can be used interchangeably. It is precisely this A_{21} that is measured by the previously mentioned angular accelerometer.

Substituting Eqs. 4, 5, and 10 into Eq. 3 yields

$$A_2 e^{j(\Omega t + \phi_{2/1})} = A_1 e^{j\Omega t} + y_{21} \alpha_x e^{j(\Omega t + \phi_{\alpha x/1})}. \quad (13)$$

Multiplying Eq. 13 through by $e^{-j\Omega t}$ leaves

$$A_2 e^{j\phi_{2/1}} = A_1 + y_{21} \alpha_x e^{j\phi_{\alpha x/1}}. \quad (14)$$

A similar development is employed when considering the motion in the z-direction of two points on a line parallel to the x-axis, points

1 and 5. Again, from Eq. 1,

$$\vec{a}_5 = \vec{a}_1 + \vec{a}_{5/1}. \quad (15)$$

Similar to Eq. 6,

$$\vec{a}_{5/1} = \vec{\alpha}_y \times \vec{r}_{15}. \quad (16)$$

The vector $\vec{\alpha}_y$, representing the angular acceleration about the y-axis, is parallel to (actually coincident with) the y-axis. The vector \vec{r}_{15} , representing the position vector of point 5 relative to point 1, is parallel to the x-axis, and therefore perpendicular to $\vec{\alpha}_y$. Therefore, Eq. 16 reduces to

$$a_{5/1} = \alpha_y r_{15}. \quad (17)$$

Unlike Eq. 8, r_{15} is defined as

$$r_{15} = x_{15} = x_1 - x_5. \quad (18)$$

This difference arises from the fact that, when following the right-hand rule convention, positive acceleration about the y-axis lifts the negative x-axis. Again considering harmonic motion,

$$\vec{\alpha}_y = \alpha_y e^{j(\Omega t + \phi_{\alpha y/1})}. \quad (19)$$

Therefore, as in Eq. 10, from Eqs. 17, 18, and 19,

$$a_{5/1} = \alpha_r r_{15} = x_{15} \alpha_y e^{j(\Omega t + \phi_{\alpha y/1})}. \quad (20)$$

As before, $a_{5/1}$ is a phasor with amplitude A_{51} such that

$$A_{51} = |x_{15}| \alpha_y. \quad (21)$$

Again, due to the absolute value sign in Eq. 21,

$$A_{51} = A_{15}. \quad (22)$$

From Eqs. 15 and 20,

$$A_5 e^{j(\Omega t + \phi_{5/1})} = A_1 e^{j\Omega t} + x_{15} \alpha_y e^{j(\Omega t + \phi_{\alpha y/1})}. \quad (23)$$

Multiplying Eq. 23 through by $e^{-j\Omega t}$ yields

$$A_5 e^{j\phi_{5/1}} = A_1 + x_{15} \alpha_y e^{j\phi_{\alpha y/1}}. \quad (24)$$

Equation 14 can be generalized for any point p on the line passing through points 1 and 2 as

$$A_p e^{j\phi_{p/1}} = A_1 + y_{p1} \alpha_x e^{j\phi_{\alpha x/1}}, \quad (25)$$

where y_p is the y coordinate of point p . Equally, Eq. 24 can be generalized for any point p on the line passing through points 1 and 5 as

$$A_p e^{j\phi_{p/1}} = A_1 + x_{1p} \alpha_y e^{j\phi_{\alpha y/1}}, \quad (26)$$

where x_p is the x coordinate of point p. At this point in the analysis, superposition is employed. Since \vec{r}_{15} and \vec{r}_{12} are orthogonal, the acceleration of any point p located anywhere in the x-y plane can be expressed as

$$A_p e^{j\phi_{p/1}} = A_1 + y_{p1} \alpha_x e^{j\phi_{\alpha x/1}} + x_{1p} \alpha_y e^{j\phi_{\alpha y/1}}. \quad (27)$$

A_1 , α_x , and α_y can be experimentally determined; and, knowing the coordinates of points 1 and p, x_{1p} and y_{p1} can be readily determined. The only remaining unknowns, $\phi_{\alpha x/1}$ and $\phi_{\alpha y/1}$, require further analysis.

5.2 Determination of Phase Angles

Dividing Eq. 14 into a real and an imaginary equation; and multiplying the imaginary equation through by $-j$, yields

$$A_2 \cos \phi_{2/1} = A_1 + y_{21} \alpha_x \cos \phi_{\alpha x/1}, \text{ and} \quad (28)$$

$$A_2 \sin \phi_{2/1} = y_{21} \alpha_x \sin \phi_{\alpha x/1}. \quad (29)$$

Squaring Eqs. 28 and 29, adding them together, and employing the relationship

$$\sin^2 \theta + \cos^2 \theta = 1 \quad (30)$$

yields

$$A_2^2 = A_1^2 + 2A_1 y_{21} \alpha_x \cos \phi_{\alpha x/1} + y_{21}^2 \alpha_x^2. \quad (31)$$

Solving Eq. 31 for $\phi_{\alpha x/1}$ yields

$$\phi_{\alpha x/1} = \cos^{-1} \left[\frac{A_2^2 - A_1^2 - y_{21}^2 \alpha_x^2}{2A_1 y_{21} \alpha_x} \right]. \quad (32)$$

Equation 32 is not a single-valued function. $\phi_{\alpha x/1}$ may be either positive or negative in sign. A similar development will show

$$\phi_{\alpha y/1} = \cos^{-1} \left[\frac{A_5^2 - A_1^2 - x_{15}^2 \alpha_y^2}{2A_1 x_{15} \alpha_y} \right]. \quad (33)$$

As in Eq. 32, Eq. 33 is not a single valued function. $\phi_{\alpha y/1}$ may be either positive or negative in sign.

Since both phase angles may each be either positive or negative, four permutations are possible,

$$(\phi_{\alpha x/1} / \phi_{\alpha y/1}) = (+/+ , +/- , -/+ , -/-)$$

Each permutation will yield a different vector \vec{a}_p , differing in phase (relative to position 1) and/or differing in amplitude. The permutations (+/+ , -/-) are found to yield the same amplitude, A_p . The remaining permutations, (+/- , -/+) generally will yield an amplitude different from that of (+/+ , -/-). Since only magnitudes are of interest only the pair of permutations yielding the proper amplitude needs to be determined. Once this choice between pairs of permutations has been made, the choice of which permutation within the

pair to use is arbitrary as each will yield the proper amplitude at any point. In practice, arbitrarily only (+/+) and (+/-) will be tested as these are representative of the two possible amplitudes. This is to say that $\phi_{\alpha x/1}$ will be taken to be positive, and that $\phi_{\alpha y/1}$ will be tested both positive and negative in Eq. 27. The resulting amplitudes are then compared to the measured levels at an arbitrary point, in this case position 6. The testing is done using the appropriate coordinates of position 6 within Eq. 27.

The foregoing analysis must be carried out for each harmonic independently. The analysis was carried out numerically, and Table 1 shows values at key points in the analysis.

5.3 Translation of Reference Point

With the foregoing analysis completed Eq. 27 now can be used to compute the motion of any point. However, generally, accelerometer position 1 is not located at the center of rotation (CR), leaving the A_1 of Eq. 27 also a function of roll and pitch. Needed is an equation of the form

$$A_p e^{j\phi_{p/CR}} = A_{CR} + f_1(\alpha_x) + f_2(\alpha_y), \quad (34)$$

since the acceleration of the center of rotation is, by definition, not a function of either α_x or α_y . Since the coordinate axes were initially chosen with the z-axis passing through the center of gravity (CG) of the compressor, the origin of the axes is the CR of the x-y plane. In order to obtain an equation on the form of Eq. 34, A_{CR} and $\phi_{CR/1}$ must be calculated using Eq. 27. The phase angles of the α 's in Eq. 34 must be referenced to the CR with the equations

TABLE 1. MOTION ANALYSIS-DEVELOPMENT

Quantity	ref eq. no.	Harmonic No.			Units
		1	2	3	
$A_1^{(1)}$		104.0	107.3	86.9	dB ⁽²⁾
A_2		108.7	104.2	81.5	dB ⁽²⁾
A_5		103.0	101.5	85.4	dB ⁽²⁾
A_{12}		111.2	102.0	88.5	dB ⁽²⁾
A_{15}		100.2	102.3	80.0	dB ⁽²⁾
A_6		107.5	93.0	78.6	dB ⁽²⁾
α_x	11	16.6	7.4	-6.1	dB ⁽³⁾
α_y	21	-0.6	1.5	-20.8	dB ⁽³⁾
$\phi_{\alpha x/1}$	32	± 136.0	± 137.8	± 153.8	deg
$\phi_{\alpha y/1}$	33	± 118.8	± 159.4	± 123.2	deg
A_6 [+/+]	27	111.5	102.4	86.6	dB ⁽²⁾
A_6 [+/-]	27	107.0	92.5	78.1	dB ⁽²⁾
Permutation Chosen		+/-	+/-	+/-	
$\phi_{CR/1}$	27	87.7	8.9	12.8	deg
A_{CR}	27	98.2	102.0	77.6	dB ⁽²⁾
$\phi_{\alpha x/CR}$	38	48.3	128.9	141.0	deg
$\phi_{\alpha y/CR}$	39	153.5 ⁽⁴⁾	-168.3	-136.0	deg

1) Quantities not indented are measured quantities
Quantities indented are derived.

2) dB ref. 1×10^{-5} m/s²

3) dB ref. 1×10^0 rad/s²

4) altered by 360° ($-180 \leq \phi \leq 180$)

$$\phi_{\alpha x/CR} = \phi_{1/CR} + \phi_{\alpha x/1}, \text{ and} \quad (35)$$

$$\phi_{\alpha y/CR} = \phi_{1/CR} + \phi_{\alpha y/1}. \quad (36)$$

Also known is the relationship

$$\phi_{1/CR} = -\phi_{CR/1}. \quad (37)$$

Combining Eqs. 25 and 36 with Eq. 37 yields

$$\phi_{\alpha x/CR} = \phi_{\alpha x/1} - \phi_{CR/1}, \text{ and} \quad (38)$$

$$\phi_{\alpha y/CR} = \phi_{\alpha y/1} - \phi_{CR/1}. \quad (39)$$

Since the axes were chosen so that

$$x_{CR} = y_{CR} = 0 \quad (40)$$

we have

$$y_{p\ CR} = y_p - y_{CR} = y_p, \text{ and} \quad (41)$$

$$x_{CR\ p} = x_{CR} - x_p = -x_p. \quad (42)$$

Substituting Eqs. 38, 39, 41, and 42 into Eq. 27 yields

$$A_p e^{j\phi_{p/CR}} = A_{CR} + y_p \alpha_x e^{j\phi_{\alpha x/CR}} - x_p \alpha_y e^{j\phi_{\alpha y/CR}}. \quad (43)$$

5.4 Analysis Implementation

All the foregoing analysis, including the translation of the

reference point, was carried out for the first three harmonics as shown in Table 1. Table 2 shows a comparison of the acceleration at each of the six accelerometer positions, to the acceleration levels determined by the describing equation, Eq. 43.

The effect of eliminating roll vibration is of considerable interest. Table 3 shows a comparison of the levels predicted by Eq. 43 under standard predicted conditions, to those where the roll component of Eq. 43 is set equal to zero. Table 4 shows a comparison of the levels predicted by Eq. 43 under standard predicted conditions, to the levels predicted by Eq. 43 if only roll is considered. Table 5 shows, additionally, a comparison of the levels predicted by Eq. 43 under standard predicted levels, to those predicted by Eq. 43 if only pitch is considered. Lastly, the levels predicted by Eq. 43 if both pitch and roll are eliminated are the same for all positions, varying only from harmonic to harmonic. These levels appear in Table 1 as A_{CR} .

TABLE 2. COMPARISON OF MEASURED AND STANDARD
PREDICTED LEVELS

Position number	Acceleration Levels, dB (re: 1×10^{-5} m/s ²)					
	Harmonic 1		Harmonic 2		Harmonic 3	
	Meas	by Eq. 43	Meas	by Eq. 43	Meas	by Eq. 43
1	104.0	104.0	107.3	107.3	86.9	86.9
2	108.7	108.7	104.2	104.2	81.5	81.5
3	101.5	101.8	105.0	104.6	85.0	85.3
4	106.3	107.0	100.0	100.3	77.6	77.7
5	103.0	103.4	101.5	101.6	85.4	85.6
6	107.5	107.2	93.0	92.6	78.6	78.6

TABLE 3. COMPARISON OF STANDARD AND NO-ROLL
PREDICTED LEVELS

Position number	Acceleration Levels, dB (re: $1 \times 10^{-5} \text{ m/s}^2$)					
	Harmonic 1		Harmonic 2		Harmonic 3	
	Std.	no-roll	Std.	no-roll	Std.	no-roll
1	104.0	102.2	107.3	105.6	86.9	81.4
2	108.7	102.2	104.2	105.6	81.5	81.4
3	101.8	98.4	104.6	102.2	85.3	77.8
4	107.0	98.4	100.3	102.2	77.7	77.8
5	103.4	92.5	101.6	96.0	85.6	74.4
6	107.2	92.5	92.6	96.0	78.6	74.4

TABLE 4. COMPARISON OF STANDARD AND ONLY-ROLL PREDICTED LEVELS

Position number	Acceleration Levels, dB (re: 1×10^{-5} m/s ²)					
	Harmonic 1		Harmonic 2		Harmonic 3	
	Std.	only-roll	Std.	only-roll	Std.	only-roll
1	104.0	105.2	107.3	96.0	86.9	82.5
2	108.7	105.2	104.2	96.0	81.5	82.5
3	101.8	104.1	104.6	94.9	85.3	81.4
4	107.0	104.1	100.3	94.9	77.7	81.4
5	103.4	105.5	101.6	96.3	85.6	82.8
6	107.2	105.5	92.6	96.3	78.6	82.8

TABLE 5. COMPARISON OF STANDARD AND ONLY-PITCH
PREDICTED LEVELS

Position number	Acceleration Levels, dB (re: $1 \times 10^{-5} \text{ m/s}^2$)					
	Harmonic 1		Harmonic 2		Harmonic 3	
	Std.	only-pitch	Std.	only-pitch	Std.	only-pitch
1	104.0	94.2	107.3	96.3	86.9	74.0
2	108.7	94.2	104.2	96.3	81.5	74.0
3	101.8	68.0	104.6	70.1	85.3	47.8
4	107.0	68.0	100.3	70.1	77.7	47.8
5	103.4	94.2	101.6	96.3	85.6	74.0
6	107.2	94.2	92.6	96.3	78.6	74.0

6. PARAMETRIC STUDY

A computer simulation of the test compressor system was developed in order to effectively conduct a parametric study. This simulation, named PABEWE, established within an interactive computing environment, includes easily understandable and convenient input and output formats. The parametric study was then conducted by selectively varying input parameters, such as connecting rod length, piston weights, etc., to the system model, PABEWE; and then tabulating the resulting output.

The interactive computing environment was IBM Corporation's Conversational Monitor System (CMS), which operates within IBM's Virtual Machine Facility/370. The computer simulation uses IBM's Continuous System Modeling Program (CSMP III, Model 3), which is based on the language Fortran IV. A sample program along with a representation output from a simulation is presented in Appendix A at the end of this report. The development of PABEWE involved several noteworthy sub-developments. These are 1) development of central equations, 2) motor model development, 3) Fourier analysis, 4) program control logic, and 5) model verification. This section is concluded by a discussion of the input parameters that were varied, and a presentation of the results of the parametric study, both contained in sub-section 6) variation of parameters.

6.1 Development of Central Equations

Roll vibration, a periodic angular acceleration, intrinsically involves torques and their reactions. Classical developments, when

analyzing torques and resulting vibrations in slider-crank type machines, typically assume that the machine does not move, and that the shaft (or rotor) revolves at a constant speed (4). The error introduced by these assumptions, while normally assumed to be tolerable, is a function of machine parameters, e.g., machine weight relative to the weight of moving components. Since these factors are to be varied, these assumptions were not made in this development, resulting in considerable complexity in the describing equations.

At this point, a few definitions are in order. The component of the motor-compressor system consisting of the motor stator, motor housing, compressor housing, and common baseplate, is referred to as the shell. The component consisting of the motor rotor, the compressor crankshaft, and the portions of the connecting rods that are attributed to the crankshaft, is referred to as the rotor. A simple representation of these components is shown in Fig. 10. All angles, θ 's, and their time derivatives will be taken as positive for counter-clockwise rotations when the machine is viewed from the compressor end as in Fig. 10. The angular displacement of the shell, θ_s , will be taken as zero when the axes of the cylinders are parallel to the z-axis. The angular displacement of the rotor, θ_R , will be taken as zero when piston 1 is at top dead center (TDC). The angular position of the rotor relative to the shell, $\theta_{R/s}$, is an important variable, termed β .

$$\beta = \theta_R - \theta_S. \quad (44)$$

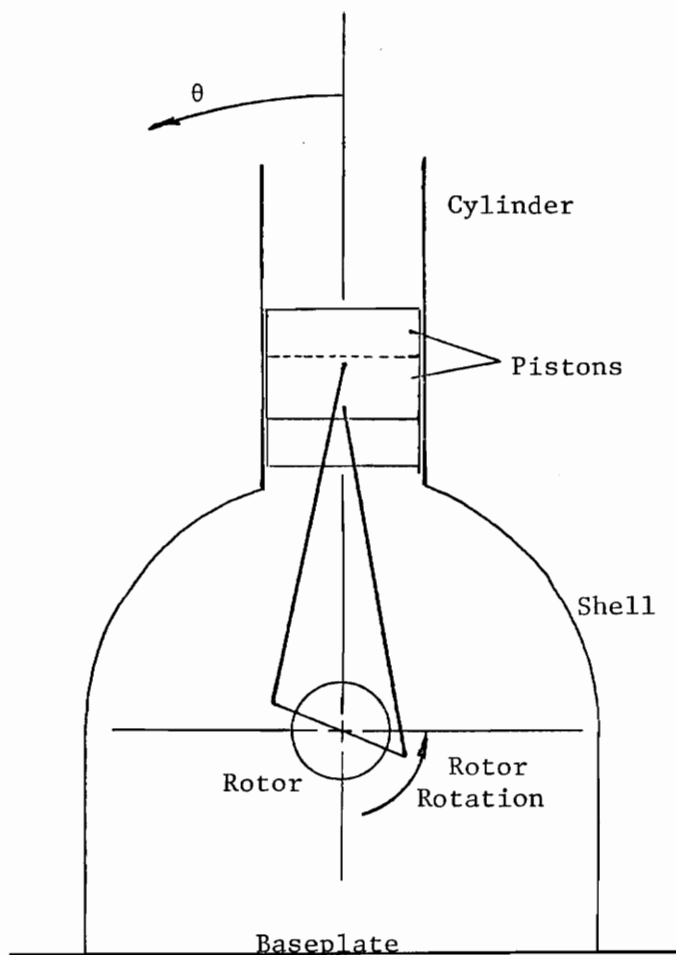


Figure 10. Schematic of Compressor Components

The pistons, differentiated by the subscripts 1 and 2, are treated as point masses as in Fig. 11. The distance from piston (mass) 1 to the rotor center line is

$$r_{M1} = R \cos \beta + L \cos \phi_1, \quad (45)$$

where R and L are the crank throw and the connecting rod lengths respectively. They are identical for pistons 1 and 2. ϕ_1 is the angle between the connecting rod and the cylinder center line, as shown in Fig. 11. By geometry, in Fig. 11,

$$R \sin \beta = L \sin \phi_1. \quad (46)$$

Solving Eq. 46 for $\sin \phi_1$,

$$\sin \phi_1 = \frac{R}{L} \sin \beta. \quad (47)$$

Using the relationship expressed in Eq. 30,

$$\cos \phi_1 = \sqrt{1 - \left(\frac{R}{L}\right)^2 \sin^2 \beta}. \quad (48)$$

Substituting Eq. 48 into Eq. 45 yields

$$r_{M1} = R \cos \beta + L \sqrt{1 - \left(\frac{R}{L}\right)^2 \sin^2 \beta}. \quad (49)$$

In order to simplify Eq. 49, the radical can be approximated by replacing it with the series (4)

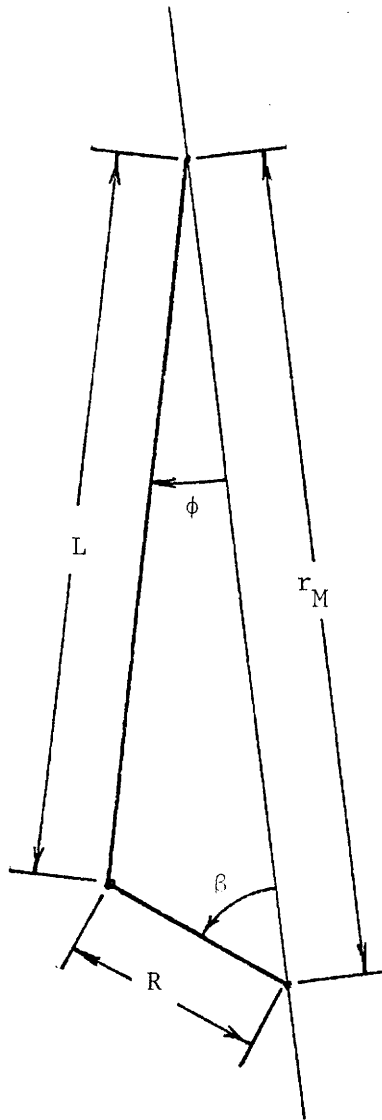


Figure 11. Geometry of the Slider-Crank Mechanism

$$(1 \pm B^2)^{\frac{1}{2}} = 1 \pm \frac{1}{2} B^2 - \frac{B^4}{2 \cdot 4} \pm \frac{1 \cdot 3 B^6}{2 \cdot 4 \cdot 6} - \frac{1 \cdot 3 \cdot 5 B^8}{2 \cdot 4 \cdot 6 \cdot 8} \pm \dots, \quad (50)$$

where

$$B = \frac{R}{L} \sin \beta. \quad (51)$$

In general it is sufficiently accurate to use only the first two terms of the series. Therefore,

$$\sqrt{1 - \left(\frac{R}{L}\right)^2 \sin^2 \beta} \cong 1 - \frac{1}{2} \left(\frac{R}{L}\right)^2 \sin^2 \beta, \quad (52)$$

and, from Eq. 49,

$$r_{M1} = R \cos \beta + L - \frac{R^2}{2L} \sin^2 \beta. \quad (53)$$

The first time derivative of r_{M1} is

$$\frac{d}{dt} r_{M1} = \dot{r}_{M1} = -R \sin \beta \frac{d}{dt} \beta - \frac{R^2}{L} \sin \beta \cos \beta \frac{d}{dt} \beta. \quad (54)$$

For convenience of nomenclature,

$$\frac{d}{dt} \beta = \dot{\beta} = \dot{\theta}_R - \dot{\theta}_S. \quad (55)$$

So Eq. 54 becomes

$$\dot{r}_{M1} = -\dot{\beta} R \sin \beta - \frac{\dot{\beta} R^2 \sin \beta \cos \beta}{L}. \quad (56)$$

Using the trigonometric identity

$$\sin \beta \cos \beta = \frac{\sin 2 \beta}{2} \quad (57)$$

Eq. 56 becomes

$$\dot{r}_{M1} = -\dot{\beta} R \sin \beta - \frac{\dot{\beta} R^2 \sin 2 \beta}{2L} . \quad (58)$$

Differentiating Eq. 53 again with respect to time, and letting

$$\frac{d}{dt} \dot{\beta} = \ddot{\beta} = \ddot{\theta}_R - \ddot{\theta}_S \quad (59)$$

we get

$$\frac{d}{dt} \dot{r}_{M1} = \ddot{r}_{M1} = -R(\dot{\beta}^2 \cos \beta + \ddot{\beta} \sin \beta) - \frac{R^2}{2L}(2\dot{\beta}^2 \cos 2\beta + \ddot{\beta} \sin 2\beta). \quad (60)$$

Since piston 2 lags piston 1 by π radians,

$$r_{M2} = R \cos(\beta - \pi) + L - \frac{R^2 \sin^2(\beta - \pi)}{2L} \quad (61)$$

Employing trigonometric identities, Eq. 61 becomes

$$r_{M2} = -R \cos \beta + L - \frac{R^2 \sin^2 \beta}{2L} . \quad (62)$$

Similarly

$$\frac{d}{dt} r_{M2} = \dot{r}_{M2} = \dot{\beta} R \sin \beta - \frac{\dot{\beta} R^2 \sin 2\beta}{2L} , \quad (63)$$

and

$$\frac{d}{dt} \dot{r}_{M2} = \ddot{r}_{M2} = -R(\dot{\beta}^2 \cos \beta + \ddot{\beta} \sin \beta) - \frac{R^2}{2L}(2\dot{\beta}^2 \cos 2\beta + \ddot{\beta} \sin 2\beta). \quad (64)$$

Equations of motion for the three component groups present, i.e., pistons, shell, and rotor, will be developed, beginning with the pistons. The conservation of angular momentum equation written for the system shown in Fig. 12, is

$$\Sigma M_0 = \frac{d}{dt} H, \quad (65)$$

where the left side of Eq. 65 is the sum of the moments about 0. The right hand is the time derivative of the angular momentum about points, H, of the piston.

$$H = I_p \dot{\theta}_s, \quad (66)$$

where I_p is the mass moment of inertia of the piston about point 0.

In equation form,

$$I_p = M_p r_M^2 \quad (67)$$

where M_p is the mass of the piston. Substituting Eqs. 66 and 67 into Eq. 65 yields

$$\Sigma M_0 = \frac{d}{dt} (M_p r_M^2 \dot{\theta}_s). \quad (68)$$

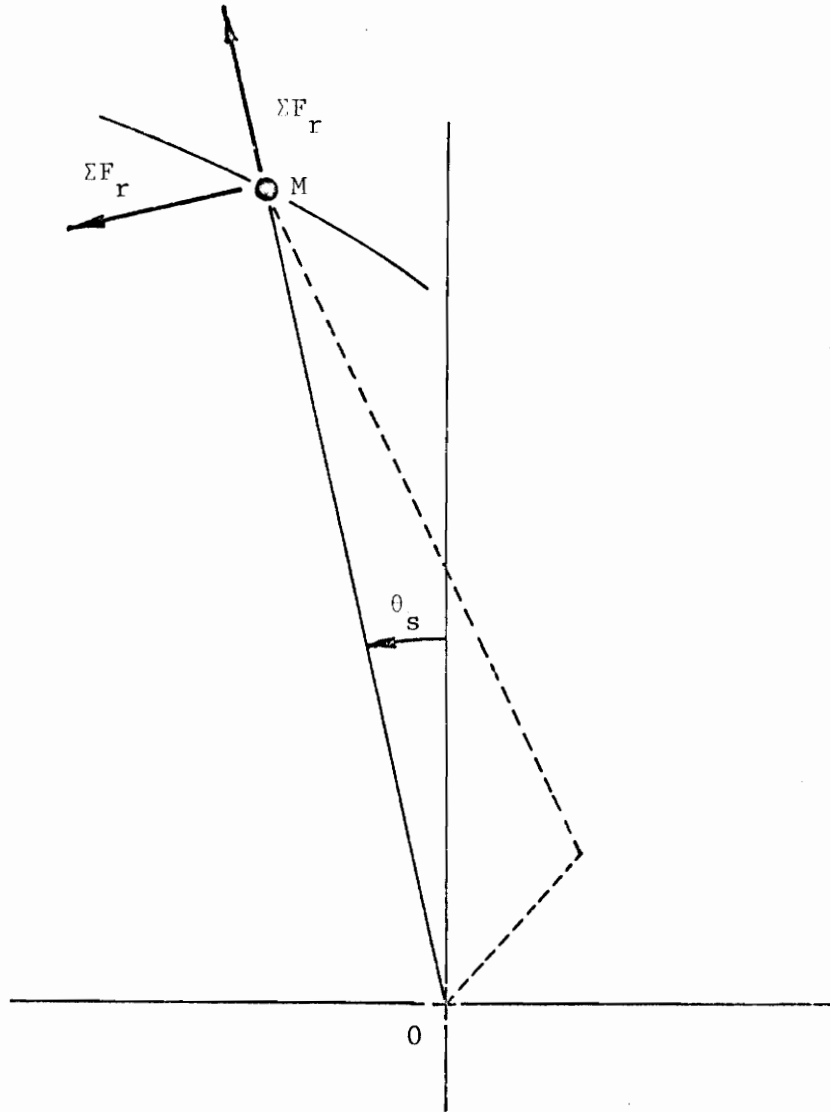


Figure 12. Piston Kinematics

Evaluating the time derivative indicated in Eq. 68 gives

$$\Sigma M_0 = M_p (r_M^2 \ddot{\theta}_S + 2 r_M \dot{r}_M \dot{\theta}_S). \quad (69)$$

Also, from Fig. 12 we have

$$\Sigma M_0 = r_M \Sigma F_\theta. \quad (70)$$

Equating Eqs. 69 and 70 and dividing through by r_M yields

$$\Sigma F_\theta = M_p (r_M \ddot{\theta}_S + 2 \dot{r}_M \dot{\theta}_S). \quad (71)$$

Also from Fig. 12, presented without proof (3) we have

$$\Sigma F_r = M_p (r_M \ddot{\theta}_S - r_M \dot{\theta}_S^2). \quad (72)$$

Consider now a freebody diagram of a piston, Fig. 13. The force between the cylinder wall and the piston, F_w , is positive in sign when imposing a counterclockwise torque on the shell and a clockwise torque on the piston (about point 0), as shown. The force between the connecting rod and the piston is taken as positive when the connecting rod is subjected to a compressive stress. The angle of the connecting rod, ϕ , also the angle of F_c , is measured as shown in Fig. 13. The force exerted on the piston by the compressed air in the cylinder, PF , is taken as positive toward the piston. (PF is not a pressure, but a force.) Summing the forces in the θ -direction yields

$$\Sigma F_\theta = -F_w - F_c \sin \phi. \quad (73)$$

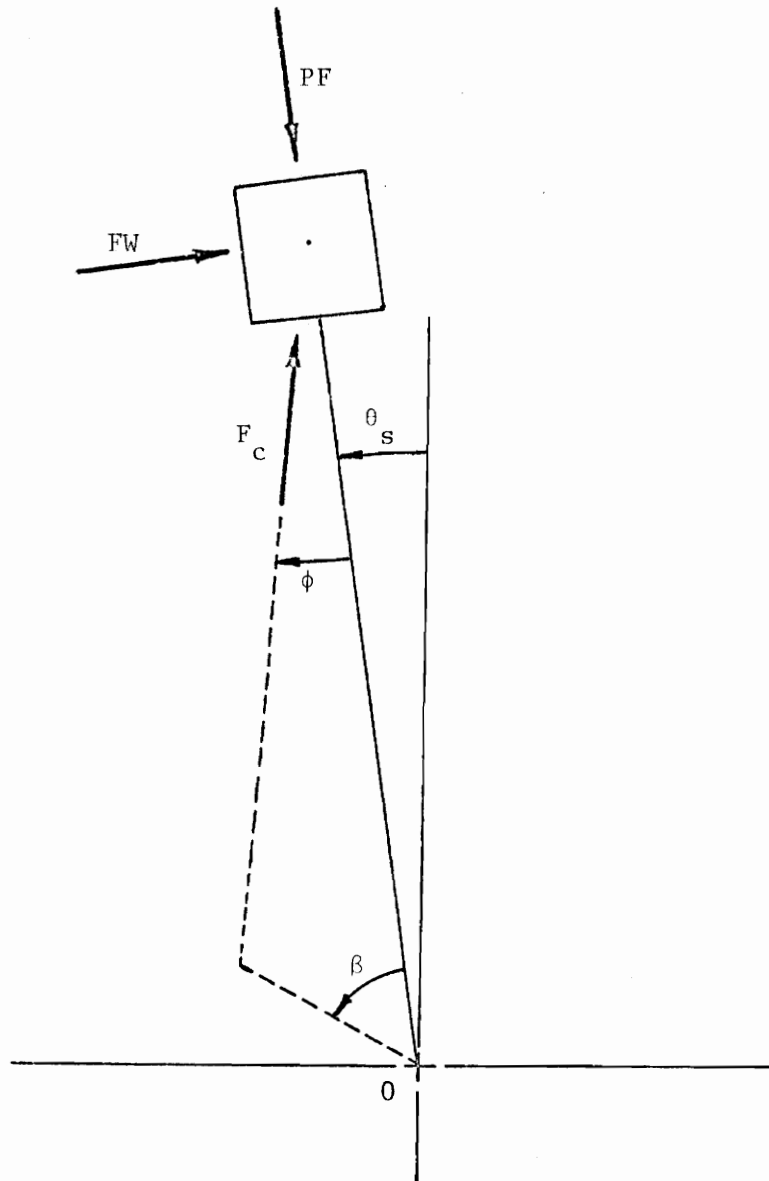


Figure 13. Free Body Diagram of Piston

Summing the forces in the r-direction yields

$$\Sigma F_r = F_c \cos \phi - PF. \quad (74)$$

Equating Eqs. 71 and 73, and solving for F_w leaves

$$F_w = -M_p (r_M \ddot{\theta}_S + 2 \dot{r}_M \dot{\theta}_S) - F_c \sin \phi. \quad (75)$$

Equating Eqs. 72 and 74, and solving for F_c leaves

$$F_c = \frac{M_p (r_M \ddot{\theta}_S - r_M \dot{\theta}_S^2) + PF}{\cos \phi}. \quad (76)$$

Substituting Eq. 76 into Eq. 75 yields

$$F_w = -M_p (r_M \ddot{\theta}_S + 2 \dot{r}_M \dot{\theta}_S) - \frac{[M_p (r_M \ddot{\theta}_S - r_M \dot{\theta}_S^2) + PF] \sin \phi}{\cos \phi}. \quad (77)$$

Consider, now, a freebody diagram of the shell, Fig. 14. The torque imposed by the resilient mounts, T_{MOUNT} , will be taken as positive when counterclockwise. The torque imposed on the shell by the motor, T_M , will be taken as positive when clockwise, as shown.

Applying Eqs. 65 and 66 to the shell leaves

$$\Sigma M_0 = \frac{d}{dt} (I_S \dot{\theta}_S). \quad (78)$$

Since the mass moment of inertia of the shell, I_S , is not a function of time,

$$\Sigma M_0 = I_S \ddot{\theta}_S. \quad (79)$$

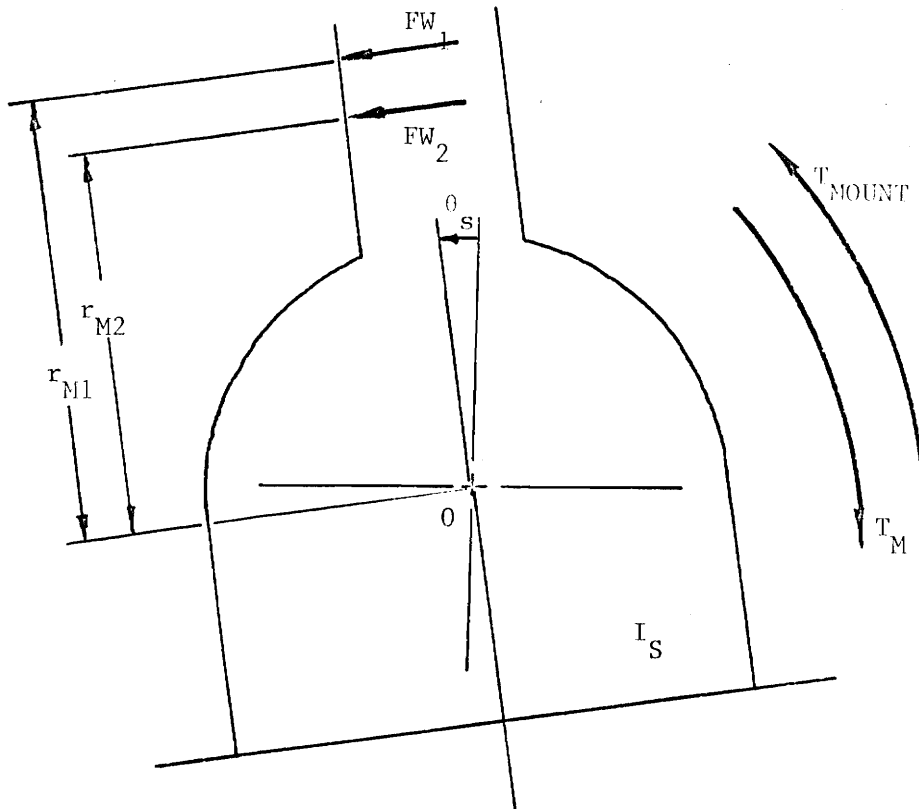


Figure 14. Free Body Diagram of Shell

Summing the moments shown in Fig. 14 yields

$$\Sigma M_0 = -T_M + T_{\text{MOUNT}} + F_{w1} r_{M1} + F_{w2} r_{M2}. \quad (80)$$

Combining Eqs. 77, 79 and 80, and solving for $\ddot{\theta}_S$ gives

$$\ddot{\theta}_S = \frac{-T_M + T_{\text{MOUNT}} - M_{P1} (r_{M1} \ddot{\theta}_S + 2\dot{r}_{M1} \dot{\theta}_S) - [M_{P1} (\ddot{r}_{M1} - r_{M1} \dot{\theta}_S^2) + PF_1] \text{TAN} \phi_1 - M_{P2} (r_{M2} \ddot{\theta}_S + 2\dot{r}_{M2} \dot{\theta}_S) - [M_{P2} (\ddot{r}_{M2} - r_{M2} \dot{\theta}_S^2) + PF_2] \text{TAN} \phi_2}{I_S} \quad (81)$$

where $r_{M1,2}$, $\dot{r}_{M1,2}$, and $\ddot{r}_{M1,2}$ are given by Eqs. 53, 62, 58, 63, 60, and 64. Equation 81 will be used later.

Consider a free-body diagram of the rotor, Fig. 15. The torques exerted on the rotor by the pistons, T_{P1} and T_{P2} , will be taken as positive when counterclockwise.

$$T_{P1} = F_{C1} R \sin(\beta + \phi_1), \text{ and} \quad (82)$$

$$T_{P2} = -F_{C2} R \sin(\beta + \phi_2). \quad (83)$$

Substituting Eq. 76 into Eqs. 82 and 83 we find

$$T_{P1} = [M_{P1} (\ddot{r}_{M1} - r_{M1} \dot{\theta}_S^2) + PF_1] \frac{R \sin(\beta + \phi_1)}{\cos \phi_1}, \text{ and} \quad (84)$$

$$T_{P2} = - [M_{P2} (\ddot{r}_{M2} - r_{M2} \dot{\theta}_S^2) + PF_2] \frac{R \sin(\beta + \phi_2)}{\cos \phi_2}. \quad (85)$$

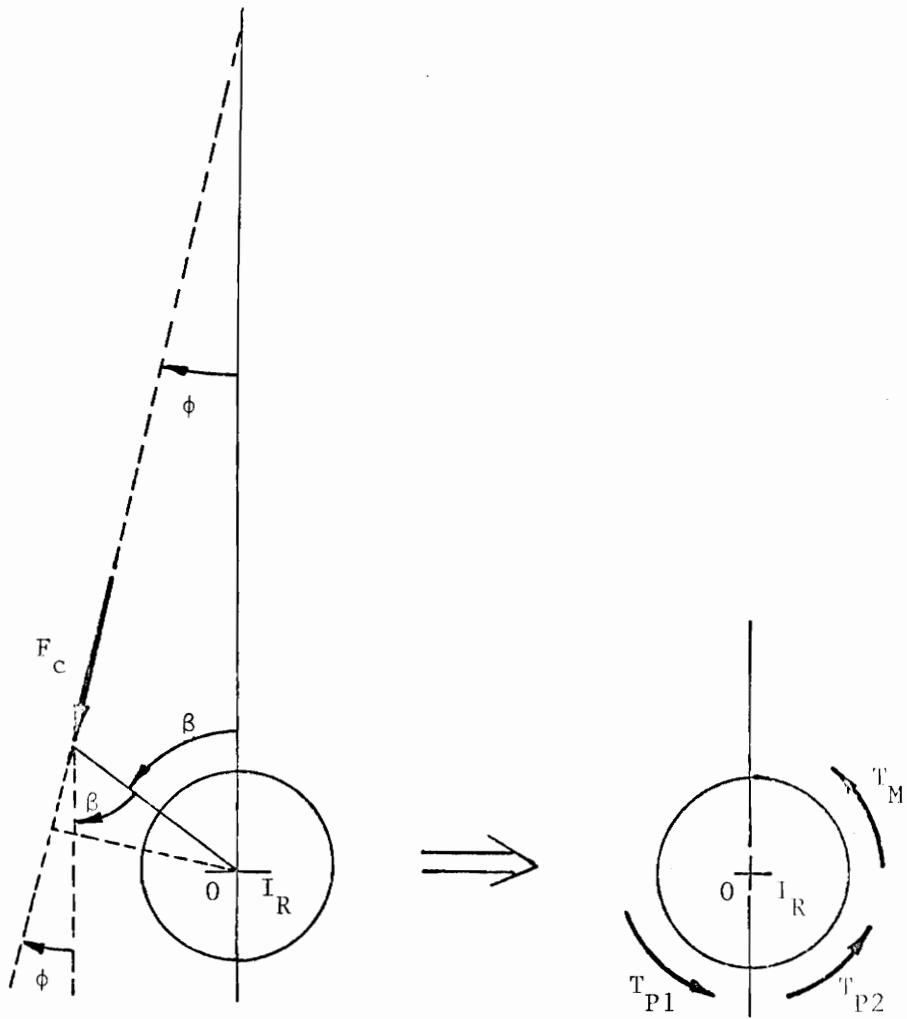


Figure 15. Free Body Diagram of Rotor

Since the mass moment of inertia of the rotor, like that of the shell, is not a function of time, Eq. 79 can be written for the rotor as

$$\Sigma M_0 = I_R \ddot{\theta}_R. \quad (86)$$

Summing the moments shown in Fig. 15 yields

$$T_{P1} + T_{P2} + T_M = I_R \ddot{\theta}_R. \quad (87)$$

Substituting Eqs. 84 and 85 into Eq. 87, and solving for $\ddot{\theta}_R$,

$$\ddot{\theta}_R = \frac{T_M + R \sin(\beta + \phi_1) [M_{P1} (\ddot{r}_{M1} - r_{M1} \dot{\theta}_S^2) + PF_1] / \cos \phi_1 - R \sin(\beta + \phi_2) [M_{P2} (\ddot{r}_{M2} - r_{M2} \dot{\theta}_S^2) + PF_2] / \cos \phi_2}{I_R}, \quad (88)$$

where $r_{M1,2}$ and $\ddot{r}_{M1,2}$ are given by Eqs. 53, 62, 60, and 64.

Equations 81 and 88 are central to this development. They are simultaneous second-order differential equations. $\ddot{\theta}_R$ and $\ddot{\theta}_S$ both occur on the right side of both equations since \ddot{r}_M is a function of $\ddot{\beta}$, where

$$\ddot{\beta} = \ddot{\theta}_R - \ddot{\theta}_S. \quad (59a)$$

In these two equations (81 and 88) only $\ddot{\theta}_R$ and $\ddot{\theta}_S$ are as yet unknowns, since $\dot{\theta}_R$, $\dot{\theta}_S$, θ_R , and θ_S can be determined by successive time integrations of $\ddot{\theta}_R$ and $\ddot{\theta}_S$. Equations 81 and 88 are two equations in two unknowns, and therefore can be solved yielding differential equations

of the form

$$\ddot{\theta}_R = f(\dot{\theta}_R, \dot{\theta}_S, \theta_R, \theta_S, R, L, \text{etc.}), \quad (89)$$

and

$$\ddot{\theta}_S = g(\dot{\theta}_R, \dot{\theta}_S, \theta_R, \theta_S, R, L, \text{etc.}). \quad (90)$$

Equations 89 and 90 are still related (for instance, $\ddot{\theta}_R$ is a function of $\dot{\theta}_S$) but are now in a form readily incorporated into a simulation program, and are central to the simulation program PABEWE of Appendix A.

6.2 Motor Model

A computer model for the motor was developed based on data supplied by the motor manufacturer. The motor is a Class B, three-phase, 440 V.A.C., squirrel-cage induction motor. The full rated output power is 44.7 kW (60.0 Hp). A table of motor speed vs. output torque was supplied with the motor, and is repeated in Table 6. This is a steady-state model, one which includes no other functional relationships such as rotor position or acceleration. For convenience,

Table 6. Motor Speed vs. Torque Data

SPEED (rpm)	TORQUE (N-m)	SLIP (rpm)	COMMENTS
900	0	0	no load
894	239	6	50% full power
889	361	11	75% full power
880	485	20	100% full power
866	616	34	125% full power
860	744	40	150% full power
830	949	70	point based on faired curve
792	1009	108	187% full power - breakdown torque
600	746	300	point based on faired curve
400	610	500	point based on faired curve
0	542	900	Locked rotor

the independent variable used in PABEWE is slip, the difference in the speed of the rotor (relative to the shell) and the electrical speed of the motor, in this case 900 rpm.

$$SLIP = 900 - 2\pi (3600) \dot{\beta}. \quad (91)$$

If the slip is negative, a negative torque is assigned as equal in magnitude to the torque associated with the slip if it were positive. Figure 16 shows a plot of the manufacturer's data with rotor speed as the independent variable. Figure 17 shows a plot of the same data but with slip as the independent variable. A portion of the curves was faired in based on characteristic curves of Class B motors. Negative torque with positive rotation comprises power generation. In fact, if an induction motor is mechanically forced to operate at a speed above the electrical speed of the impressed voltage, it will generate electrical power.

This motor model was input to PABEWE as a series of data points along with the appropriate logic to handle negative input values of slip. These data points are then interpolated based on the quadratic interpolation capability of CSMP. This motor model was easily integrated into the total program PABEWE.

6.3 Fourier Analysis

CSMP has many graphic and tabular output formats available as standard options for the user. However, these all comprise some system variable being plotted or tabulated as a function of the

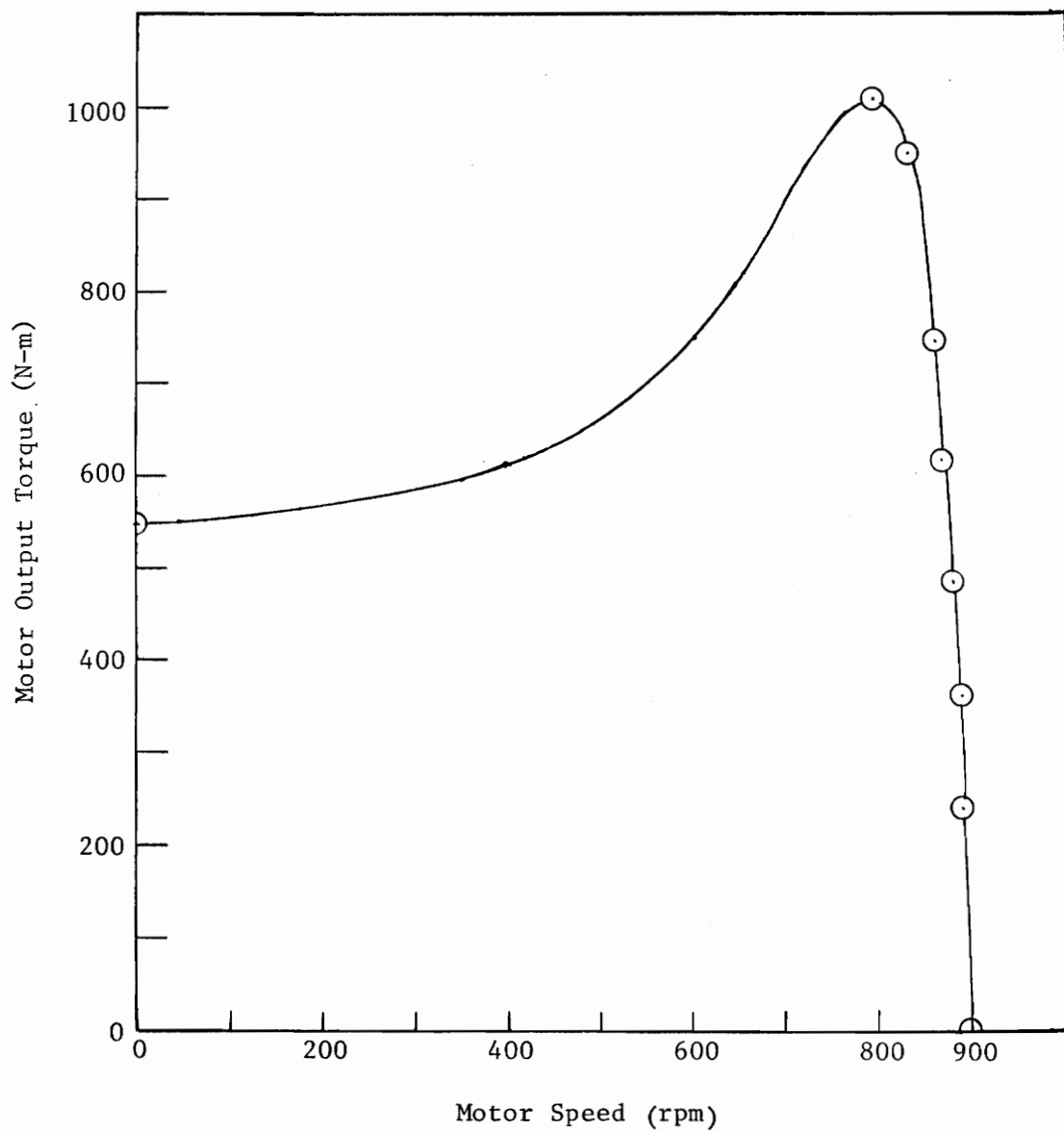


Figure 16. Test Motor Characteristic Curve

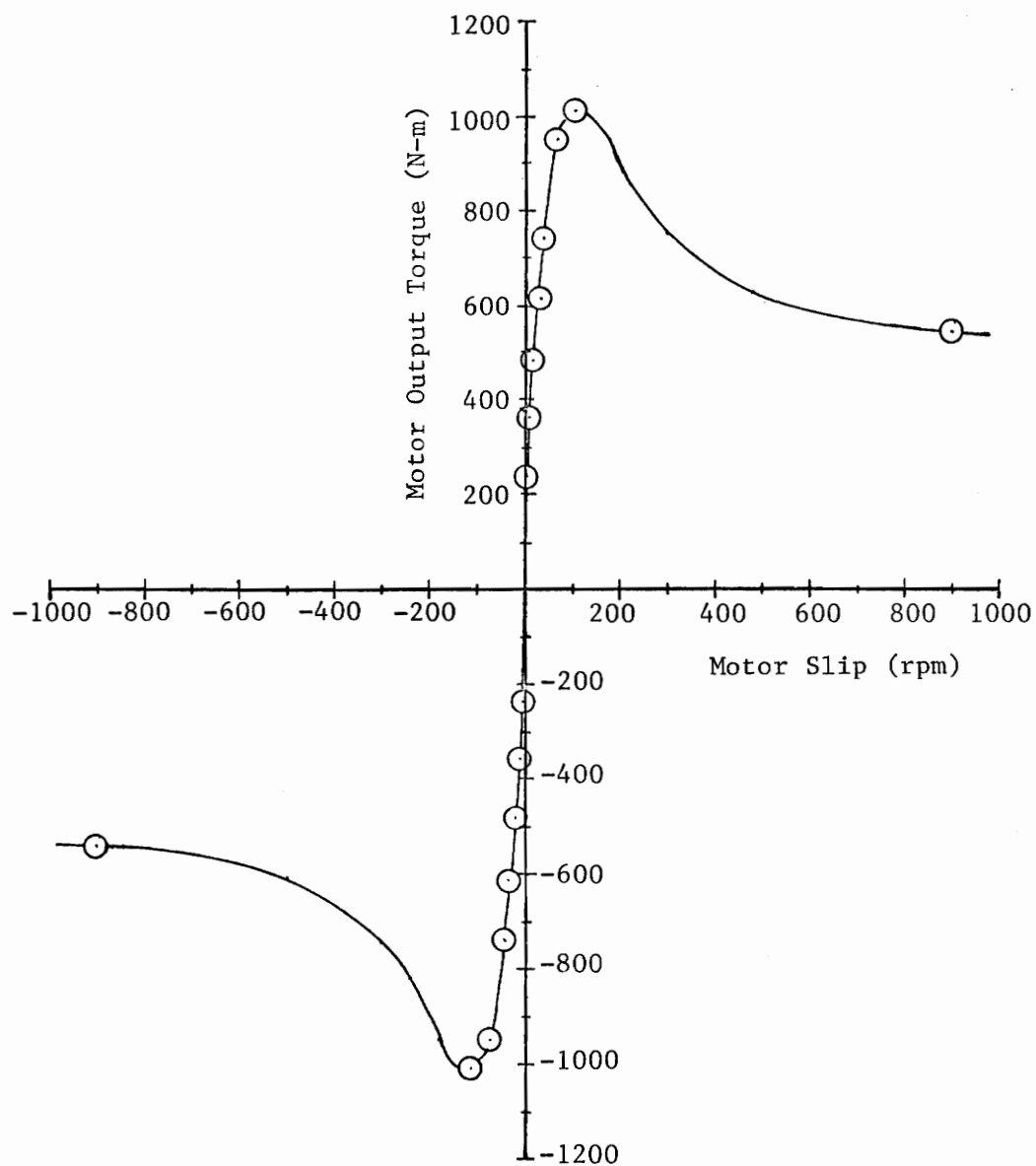


Figure 17. Motor Characteristic Curve as Input to PABEWE

independent variable, time. The most useful output form for engineers is the presentation of the system variables as a function of frequency, or, more explicitly, the Fourier coefficients of these system variables at harmonics of the base rotational frequency. Therefore, it was decided to use the integration facility of CSMP to generate the needed Fourier coefficients.

The Fourier series for a periodic function $f(t)$ satisfying certain continuity conditions is

$$f(t) = A_0 + \sum_{n=1}^{\infty} A_n \cos\left(\frac{2\pi nt}{P}\right) + \sum_{n=1}^{\infty} B_n \sin\left(\frac{2\pi nt}{P}\right), \quad (92)$$

where P is the period of the function $f(t)$, n is the harmonic number, and where A_n and B_n are utilized to calculate the Fourier coefficients of interest. Specifically, the magnitudes of the Fourier coefficients are

$$C_n = \sqrt{A_n^2 + B_n^2}, \quad (93)$$

and the phase angles of the Fourier coefficients are

$$\phi_n = \tan^{-1} \left(\frac{B_n}{A_n} \right) \quad 0 \leq \phi_n \leq 2\pi. \quad (94)$$

The terms A_n and B_n are defined by

$$A_n = \frac{2}{P} \int_a^{a+P} f(t) \cos\left(\frac{2\pi nt}{P}\right) dt, \quad \text{and} \quad (95)$$

$$B_n = \frac{2}{P} \int_a^{a+P} f(t) \sin\left(\frac{2\pi nt}{P}\right) dt. \quad (96)$$

Therefore, to calculate ten Fourier coefficients (C_n), twenty integration statements are needed in the CSMP program. These Fourier coefficients are then converted to decibels, and are then directly comparable to experimental data obtained from the actual motor-compressor system utilizing a real time analyzer (RTA) for data reduction. While several system variables were thus analyzed, the analysis was generally applied to $\ddot{\theta}_S$.

CSMP is not actually a continuous simulation, but rather it operates at discrete time intervals, or steps. These time steps, while they may be small, are finite. Therefore, the period of the function input to the Fourier analysis, P , can only be estimated to within one time step. The accuracy with which the period P can be estimated is proportional to the number of time steps the program executes per simulated revolution of the compressor. For ± 1 per cent accuracy, at least 100 equal length time steps must be taken.

To determine the period estimation accuracy required for an acceptable accuracy of the Fourier coefficients, a test computer program was devised. A program containing only the Fourier analysis was developed, with a square wave function as input. The period was known precisely, but was varied to simulate inaccuracy in period estimation. It was found that, for the first ten harmonics, a period estimation accuracy of ± 1 per cent yielded less than 0.5 dB error in the Fourier coefficients calculated. As a result, a time step size of 0.5 mS was adopted providing typically 136 time steps per revolution of the compressor.

The ten levels calculated by PABEWE were tabulated in an easily readable output format. These levels, and their phase angles are shown at the end of Appendix A for a typical simulation.

6.4 Program Control Logic

The Fourier analysis imposes the requirement of stable operation, on the simulation. This requirement stems from two considerations. First, the angular acceleration of the shell, $\ddot{\theta}_S$, must be periodic, without transients, to assure repeatability of data. Second, the period of $\ddot{\theta}_S$, which is the time for one rotor revolution, must be constant since the period P used in the Fourier analysis is the period of the revolution prior to the revolution that is analyzed. Stable operation is determined by the following method. The program continuously monitors β for the passing of multiples of 2π . The time difference between these passings is computed. When this difference, i.e., period, differs from the period of the previous cycle by less than a prescribed percentage, PRDERR, the system is termed stable. Once the system is stable, the Fourier integrators are activated, and the simulation is permitted to continue for exactly one more cycle.

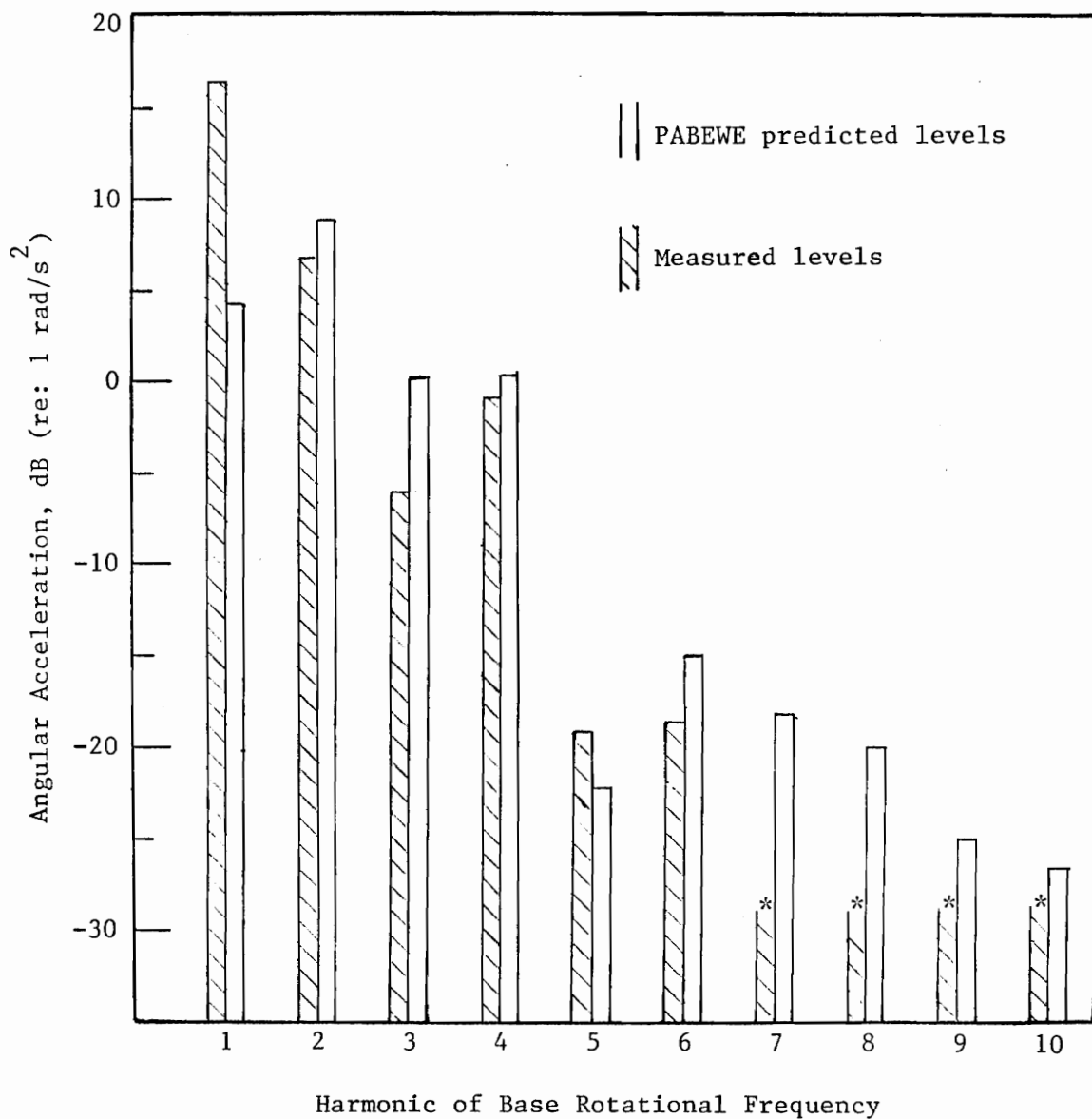
From this description of the central control logic it is apparent that the minimum number of revolutions per successful simulation is three; two to calculate two successive periods and be termed stable, and one more for the Fourier analysis. Although the time permitted for a simulation, 0.50 sec, allowed for about seven revolutions, the

simulation, when operating properly, never required more than the minimum of two revolutions to stabilize. Since the chosen time-step size permitted about 136 time-steps per revolution, the stability criterion, PRDERR, was typically set as 1 per cent. Had the compressor model not achieved stable operation within 0.5 s, as was the case in several incorrect simulations, the Fourier integrators would not have been activated, and a message to that effect would have been printed to the user.

6.5 Model Verification

Having fully developed the computer model PABEWE, it was appropriate to verify that it truly modeled the test motor compressor system. In addition to the stability constraint one valid model, it was realized that the total angular momentum, H , of the motor compressor system as modeled) must remain constant. Therefore, the initial and final total angular momentums are compared. If they differ by greater than 0.1 per cent, a warning is issued to the user. Typical values for this variation are ± 0.003 per cent.

The primary and most obvious verification arises from a comparison of the vibration levels measured and the levels predicted by PABEWE under best guess conditions, i.e., all input parameters are those of the test compressor. Figure 18 shows this comparison. While there are considerable differences in the levels, the model was judged to be adequate for the parametric study.



* Levels not recorded

Figure 18. Comparison of Measured and PABEWE Predicted Levels

Here it is appropriate to discuss the mounts and their omission from this model. Late in this study the mounts were modeled and integrated into PABEWE. The inclusion of the mounts changed only the first harmonic significantly (4.3 to 72. dB). Therefore, it was felt that the results of the parametric study remained credible and useful. The inclusion of the mounts in PABEWE caused severe start-up transients equivalent to the compressor rocking on its mounts. These transients rendered the stability criterion (based on compressor speed) ineffective at assuring valid roll vibration levels. Depending on the damping modeled for the mounts, the program required logic to force it to run for typically twenty to thirty revolutions before valid roll vibration levels could be calculated. The duration of this transient was also determined by how close to actual running conditions the simulation was started. While inclusion of the mounts somewhat improved the ability of PABEWE to model the test compressor, it was felt that the results of the parametric study remain credible and useful.

6.6 Variation of Parameters

The computer model PABEWE was utilized to study the effects of variation of system parameters on rotational acceleration levels of the motor-compressor system. Parameters chosen for this study were:

- a) compressor connecting rod length, b) compressor crank throw length,
- c) shell inertia, d) rotor inertia, e) compressor piston mass, and
- f) compressor piston forces. The general conclusion from these

studies is that the variation of these parameters, except the piston pressure forces, within physically realizable limits will not result in large reductions of rotational acceleration levels.

Connecting Rod Length

The effect of the variation of the compressor connecting rod length from the actual value of 292.1 mm (11.5 in.) is shown in Fig. 19. The number on the right of the figure indicates the number of the harmonic plotted. (Only the six highest harmonics have been plotted.) For example, it is seen that the second harmonic has the highest acceleration levels over the range studied. The dashed line indicates the acceleration levels for the actual connecting rod length of 292.1 mm (11.5 in.). The abscissa is a logarithmic scale allowing the entire range of connecting rod lengths investigated to be represented. As can be seen in Fig. 19, reductions of the connecting rod length below 292.1 mm (11.5 in.) result in a slight increase of most of the levels. Increases of the connecting rod length result, in all but the fifth harmonic, in a decrease in the acceleration levels. However, to obtain a 10 dB reduction in the second (highest) harmonic, a connecting rod length of approximately 3302 mm (130 in.) is required. A 6 dB decrease requires a connecting rod length of approximately 1930 mm (76 in.). Neither of these changes are physically realizable. The results are seen to be similar for the other harmonics.

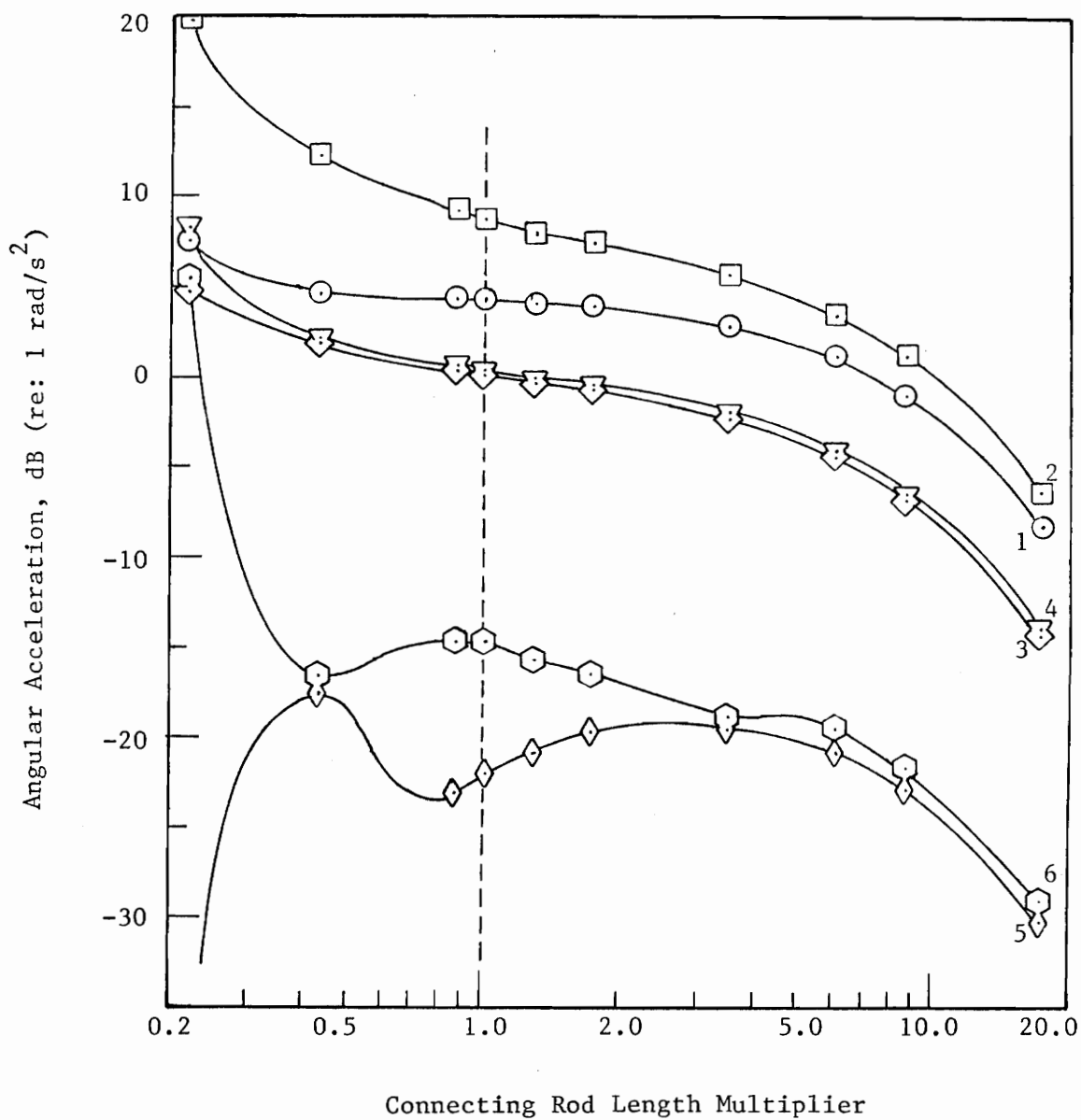


Figure 19. Effect of Connecting Rod Length on the Angular Acceleration of the Shell

Crank Throw Length

The effect of crank throw length on rotational acceleration levels is shown in Fig. 20. Here, increases of the crank throw length from the actual length of 63.5 mm (2.5 in.) result in higher levels of rotational acceleration. Decreases of the crank throw length result in a decrease of the acceleration levels. However, large changes in crank throw length are required for significant acceleration reductions. For example, to obtain a 10 dB reduction a crank throw length of 21 mm (0.8 in.) is required; and a 6 dB reduction requires a crank throw length of 32 mm (1.3 in.). The latter change of 2:1 in the crank throw length may be physically realizable.

Shell Moment of Inertia

The effect of shell moment of inertia on the rotational acceleration levels was also investigated. It was expected that a "heavier" shell would result in lower shell acceleration levels, and this was the result obtained. Figure 21 shows the levels expected for differing shell moment of inertias. The best estimate of the actual shell moment of inertia about the x-axis is 152 kg-m^2 (3600 lbm-ft^2); and for a 10 dB reduction of the second harmonic a shell moment of inertia of approximately 464 kg-m^2 ($11,000 \text{ lbm-ft}^2$) is needed. For a 6 dB reduction a shell moment of inertia of 304 kg-m^2 (7200 lbm-ft^2) is needed. These increases in shell moment of inertia are physically realizable; however they may not be desirable in service.

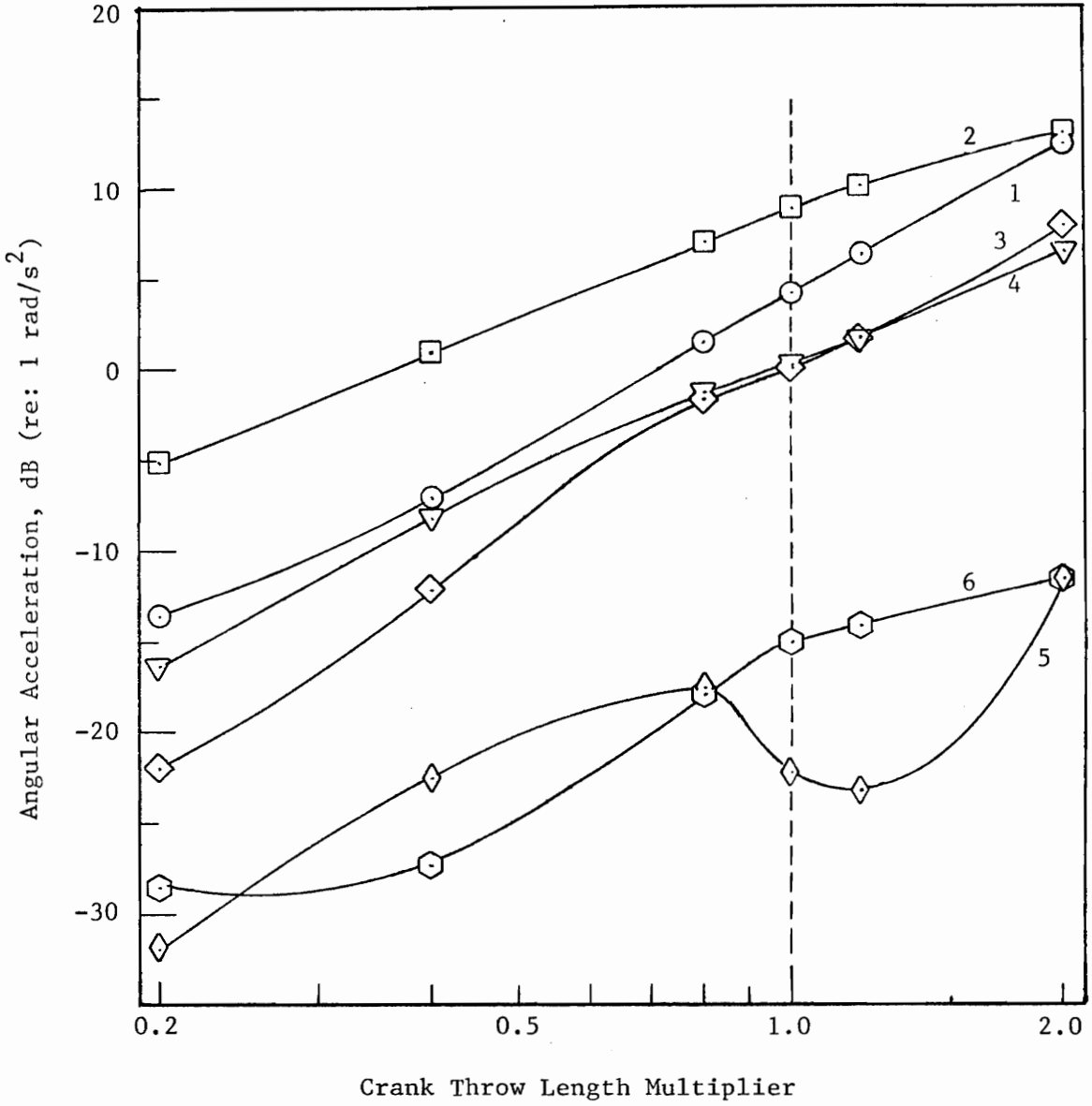


Figure 20. Effect of Crank Throw Length on the Angular Acceleration of the Shell

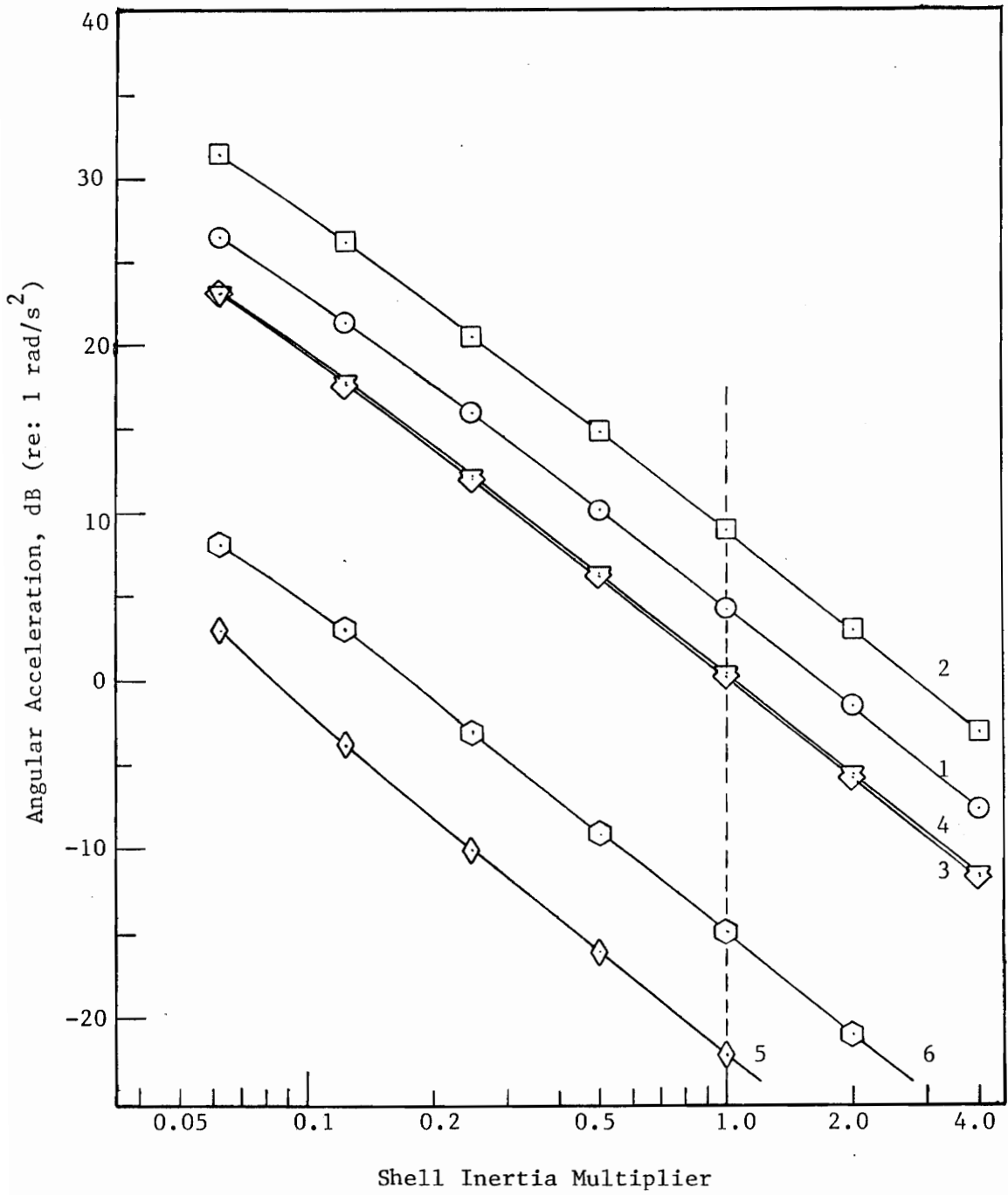


Figure 21. Effect of Shell Moment of Inertia on the Angular Acceleration of the Shell

Rotor Moment of Inertia

The effect of changes in the rotor moment of inertia are opposite to those of the shell moment of inertia. Figure 22 shows these results. Reductions of the rotor moment of inertia below the best estimate value of 2.1 kg-m^2 (50 lbm-ft^2) result in shell acceleration level reductions for the two highest harmonics. For example, if the rotor moment of inertia is reduced to 0.3 kg-m^2 (6 lbm-ft^2) the acceleration levels of the second, first, fourth, and third harmonics are reduced by 10 dB, 8.5 dB, 2.4 dB, and 5 dB, respectively. However, strength considerations will most likely prevent large decreases in the rotor moment of inertia.

Piston Mass

The effect of piston mass was also investigated. The piston weights comprising best estimate weights used in PABEWE are made up of the weight of the individual pistons plus a portion of the connecting rods' masses. This portion was determined by the equivalent mass method (4). The moments of inertia of the connecting rods, a necessary input to this method, were determined by a standard laboratory pendulum technique.

Figure 23 shows the effect of varying both piston masses by the same factor. As can be seen, the acceleration levels for the second and sixth harmonics reach minima at a multiplication factor of approximately 2.0 with the first, third, and fourth harmonics remaining relatively constant to that point. The reduction of the

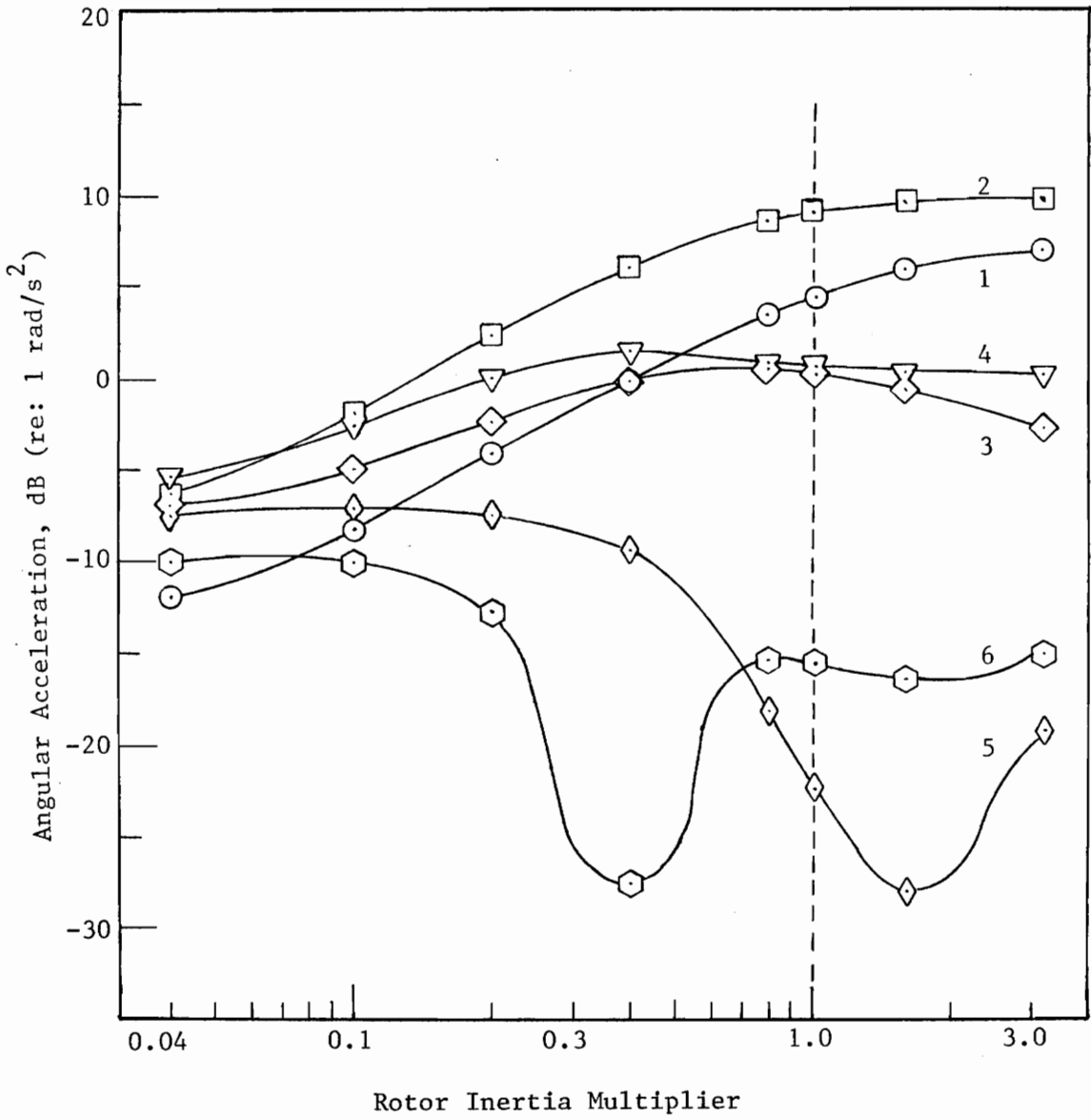


Figure 22. Effect of Rotor Moment of Inertia on the Angular Acceleration of the Shell

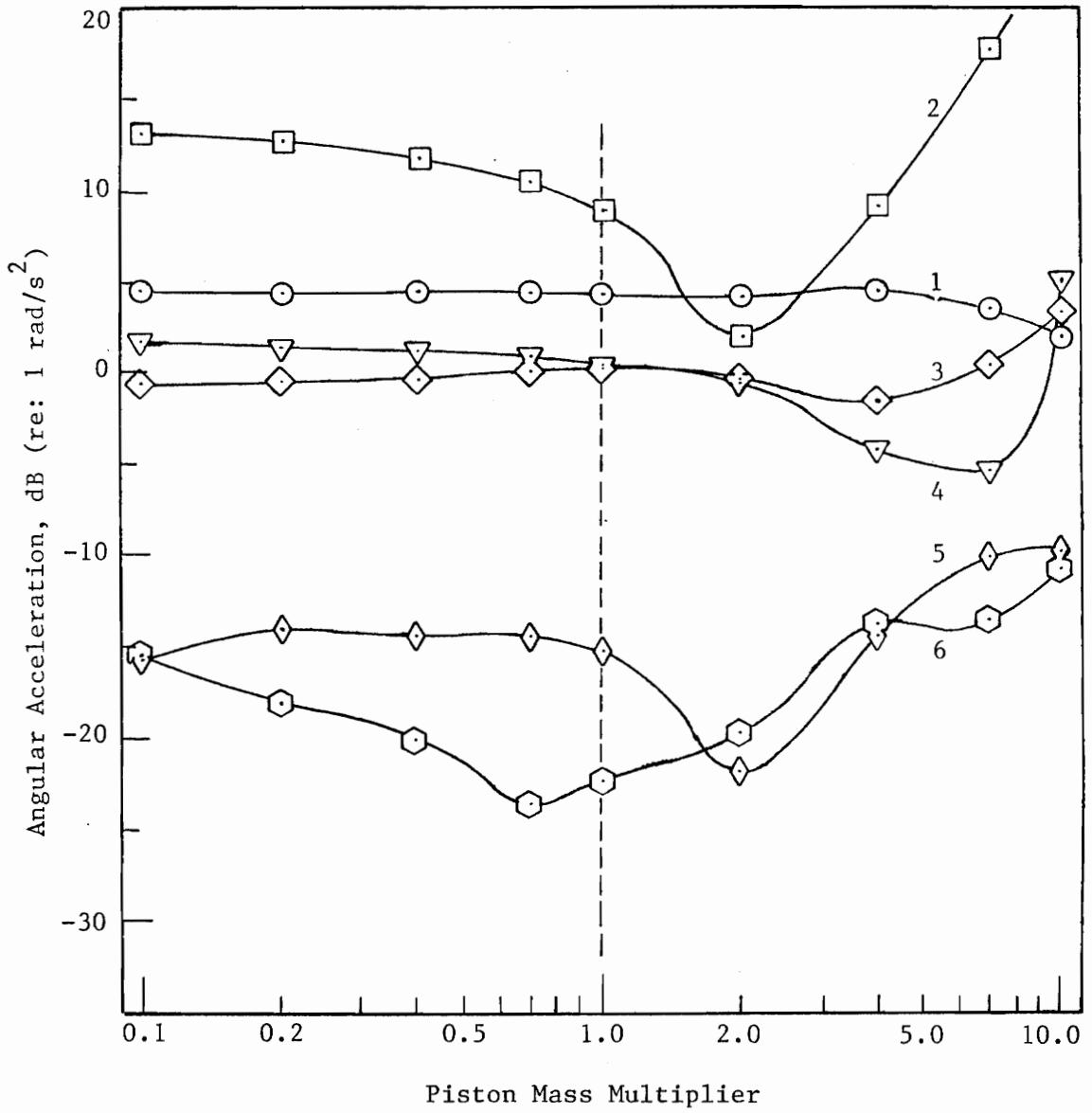


Figure 23. Effect of Piston Mass on the Angular Acceleration of the Shell

second harmonic for a factor of 2.0 is 7 dB. Studies have been conducted with independent variation of each of the piston masses. The results are similar to those presented in Fig. 23. However, the minima for the second and sixth harmonic are shifted to a multiplication factor, for one piston, of approximately 4.0. These increases in piston mass seem to be physically realizable. However, their effect on pure z-direction acceleration levels has not been investigated.

Piston Pressure Force Relationships

The piston pressure forces assumed for the PABEWE model comes from manufacturer's data from a similar compressor. A study was conducted where these pressures were varied from the best estimate values. In this study, the pressure forces were assumed to be equal on both pistons (with piston 2 lagging piston 1 by 180 degrees, of course). This condition may not be physically possible. However, very large reductions of the odd-numbered harmonics of the acceleration levels of the shell resulted. These data are shown in Table 7.

These effects are seen to indicate that variations in the piston pressure forces may result in significant reductions of the rotational acceleration levels of the shell.

Table 7. Effect of Equal Piston Pressure Forces on Angular Acceleration of the Shell

Harmonic	Acceleration Levels, dB (re: 1×10^0 rad/s ²)	
	best estimate	equal pressure forces
1	4.3	-38.7
2	8.9	4.2
3	0.2	-50.1
4	0.4	-0.4
5	-22.2	-42.0
6	-15.0	-25.7
7	-18.2	-53.2
8	-20.0	-22.9
9	-25.0	-59.2
10	-26.6	-26.2

7. CONTROL OF ROLL VIBRATION

One of the major goals of this work has been the reduction of the roll mode of vibration present in the motor-compressor system. After identifying the contribution that roll vibration made to the overall vibration spectrum it was decided to employ classical automatic control methods to reduce this vibration. This section presents

- 1) the reduced-order model utilized in the control design study, and
- 2) the results of the control design.

7.1 Development of Reduced-Order Equations

The complete model equations, as contained in the PABEWE simulation, were very cumbersome for use in a control system design. Therefore, the equations were reduced utilizing reasonable approximations. The reduced equations are shown in block diagram form in Fig. 24. K_M is the assumed linear slope of the motor slip characteristic shown in Fig. 17. K_M is termed the motor gain. The function $f(\theta_R)$, based on an average rotor speed, is the only non-linear term in the model, and accounts for the slider-crank nonlinearities as well as the piston pressure forces. The angular acceleration levels, $\ddot{\theta}_S$, predicted by these reduced equations, using best-estimate values, are within ± 1.1 dB of the levels predicted by the PABEWE simulation.

An attempt was made to effect a control design utilizing the describing function technique(5). The describing function was needed

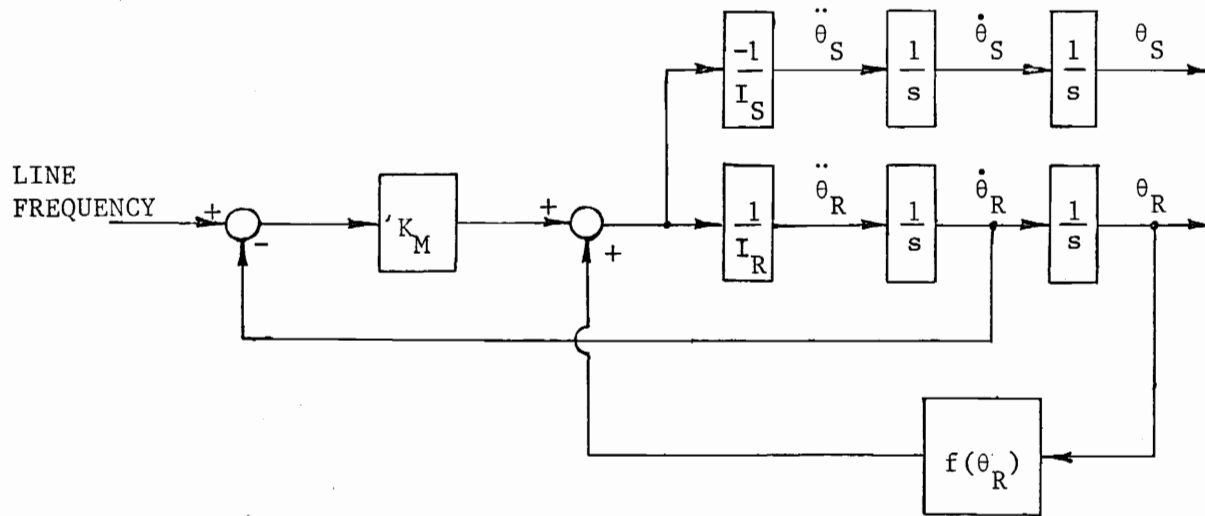


Figure 24. Block Diagram of Simplified Model of Roll Dynamics

to include the nonlinear term $f(\theta_R)$. However, it was not possible to characterize $f(\theta_R)$ with a describing function. Two extensive literature reviews in this area revealed no previous work that would be of any aid. Therefore, the describing function approach was discarded.

The next approach was to treat the feedback signal $f(\theta_R)$ as a disturbance. Since the speed of the rotor varied by typically less than 4.0 %, the position of the rotor, θ_R , could be approximated by a ramp function of time. Inputting this ramp function of time into the nonlinear $f(\theta_R)$ yielded a cyclic disturbance torque, $d(t)$, and yielded the model shown in Fig. 25. This simplification, while it did not significantly alter the simulation, provided a model easily evaluated by standard control techniques. For the purposes of the control studies presented in the following section, the function $d(t)$ was approximated by a three-term Fourier series consisting of a constant and the first two harmonic components. The $d(t)$ utilized for this control system design is

$$f(\theta_R) \cong d(t) = -303.3 + 352.6 \cos(\Omega t + 271^\circ) \\ + 488.2 \cos(2\Omega t + 64.7^\circ) \text{ N-m. (97)}$$

7.2 Control System Design

Two feedback variables and a controller gain were added to the system for the design studies. Feedback from the angular acceleration of the shell, $\ddot{\theta}_S$, and the angular velocity of the rotor, $\dot{\theta}_R$, was utilized. The controller added to the model is a representation of

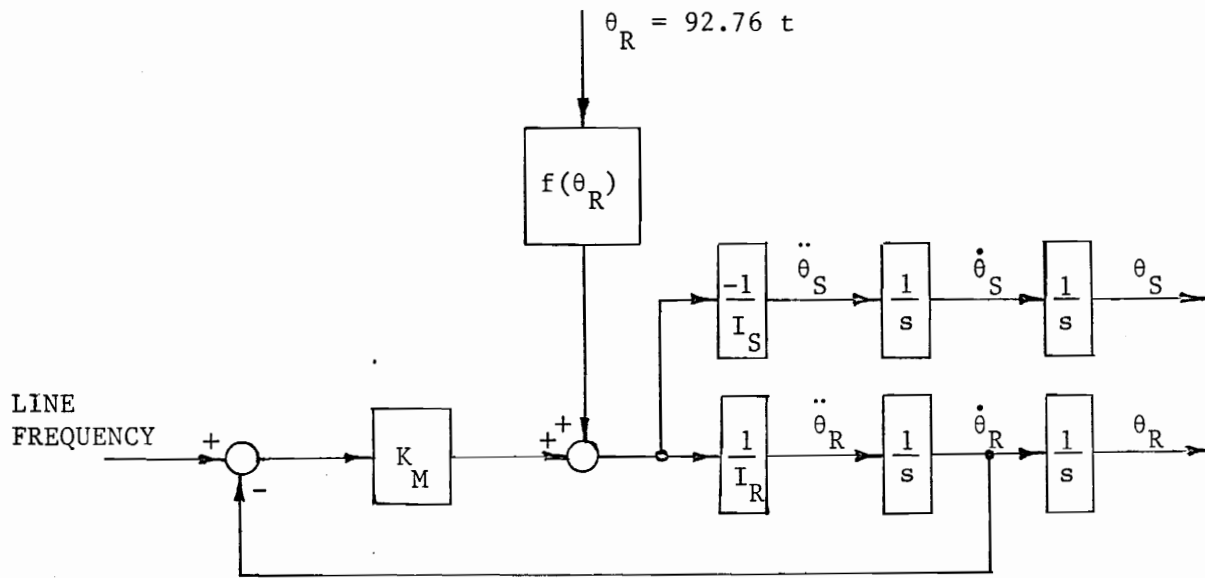


Figure 25. Block Diagram of Simplified Model of Roll Dynamics
With Disturbance Input

a variable frequency controller utilized for speed control of a.c. synchronous and induction machines. Figure 26 shows a block diagram of the system with the feedback and the controller added. K is the assumed linear controller gain, $k_{\theta_S}^{\cdot\cdot}$ is the feedback coefficient for the angular acceleration of the shell, and $k_{\theta_R}^{\cdot}$ is the feedback coefficient for the angular velocity of the rotor. R is the system reference input. Solving for $\dot{\theta}_R$ we get

$$\dot{\theta}_R(s) = \frac{d(s) + K K_M R(s)}{(I_R - K K_M \frac{I_R}{I_S} k_{\theta_S}^{\cdot\cdot})s + (K K_M k_{\theta_R}^{\cdot} + K_M)} \quad (98)$$

These three parameters, $k_{\theta_R}^{\cdot}$, $k_{\theta_S}^{\cdot\cdot}$, and K , can be varied to obtain a reduction in roll vibration levels. In addition this model may be utilized to examine the effects of changing the motor gain, K_M .

The nominal steady-state rotor speed, $\dot{\theta}_R$, is a function of R , K , K_M , and $k_{\theta_R}^{\cdot}$. Assuming the speed is not to be significantly changed in the controller case, a constraint will have to be placed on one or more of these parameters to realize the unchanged speed. An analytical expression for the nominal steady-state speed can be derived by assuming the oscillating (harmonic) components of $d(t)$ to be zero and utilizing the final value theorem of Laplace transforms.

$$\dot{\theta}_R \Big|_{ss} = \lim_{s \rightarrow 0} s(\dot{\theta}_R(s)). \quad (99)$$

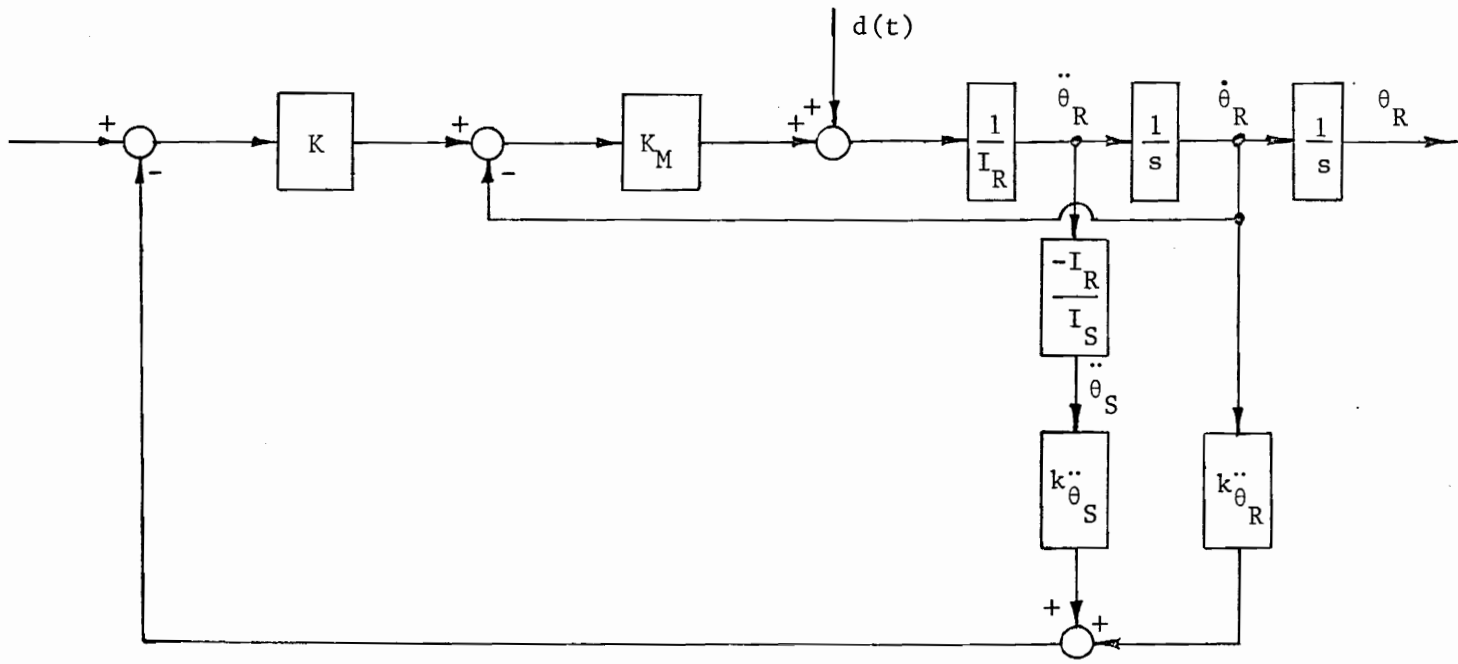


Figure 26. Block Diagram of Simplified Model of Roll Dynamics
With Added Feedback

Substituting Eq. 98 into Eq. 99 yields

$$\dot{\theta}_R \Big|_{ss} = \lim_{s \rightarrow 0} s \left[\frac{d(s) + K K_M R(s)}{(I_R - K K_M \frac{I_R}{I_S} k_{\theta_S}^{\ddot{\cdot}})s + (K K_M k_{\theta_R}^{\dot{\cdot}} + K_M)} \right]. \quad (100)$$

Assuming

$$R(t) = 15 \text{ Hz} = 94.25 \text{ rad/s}. \quad (101)$$

Therefore,

$$R(s) = \frac{94.25}{s}. \quad (102)$$

Eliminating the harmonic components from $d(s)$ we have

$$d(s) \approx -\frac{303.3}{s}. \quad (103)$$

Substituting Eqs. 102 and 103 into Eq. 100 and evaluating the limit yields

$$\dot{\theta}_R \Big|_{ss} = -\frac{303.3 + K K_M (94.25)}{K K_M k_{\theta_R}^{\dot{\cdot}} + K_M}. \quad (104)$$

Dividing Eq. 104 through by $K K_M$ gives

$$\dot{\theta}_R \Big|_{ss} = \frac{\frac{-303.3}{K K_M} + 94.25}{k_{\theta_R}^{\dot{\cdot}} + 1/K}. \quad (105)$$

The case of no feedback control corresponds to the condition of

$$K = 1, \text{ and } k_{\dot{\theta}_R} = k_{\ddot{\theta}_S} = 0.$$

For this condition, using a best-estimate value of $K_M = 203.4 \frac{\text{N-m-s}}{\text{rad}}$, we find

$$\dot{\theta}_R \Big|_{ss} = 92.76 \text{ rad/s} = 14.76 \text{ Hz.} \quad (106)$$

Using this speed as a "target" speed for our design, a relation between $k_{\dot{\theta}_R}$ and K was derived to be

$$k_{\dot{\theta}_R} = 1.016 (1 - K^{-1}). \quad (107)$$

Therefore, it is seen that for any value of K chosen, a corresponding value of $k_{\dot{\theta}_R}$ can be chosen to keep the rotor speed at the target speed. For a target speed of 92.76 rad/s, as K approaches large values, $k_{\dot{\theta}_R}$ approaches 1.016.

The next step is to determine the values of K and $k_{\ddot{\theta}_S}$ for roll vibration reduction. The expression for $\ddot{\theta}_S$ can be found from Eq. 98 utilizing the expression

$$\ddot{\theta}_S = -\frac{I_R}{I} \ddot{\theta}_R = \left(-\frac{I_R}{I_S} s\right) \dot{\theta}_R. \quad (108)$$

Therefore,

$$\ddot{\theta}_S = \frac{(-\frac{I_R}{I_S} s)(d(s) + K K_M R(s))}{(I_R - K K_M \frac{I_R}{I_S} k_{\theta_S}^{\cdot\cdot})s + (K K_M k_{\theta_R}^{\cdot} + K_M)} \quad (109)$$

To examine the angular acceleration of the shell consider only the harmonic components of the input, $R(t)$, and the disturbance, $d(t)$. $R(t)$ has no harmonic components. The harmonic components of $d(t)$ are, from Eq. 97,

$$d(t) \Big|_{\text{HARMONIC}} \cong 352.6 \cos(\Omega t + 271^\circ) + 488.2 \cos(2\Omega t + 64.7^\circ) \text{ N - m.} \quad (110)$$

Each harmonic component will be treated separately; and the phase angle information will be dropped. The amplitude of oscillation of $\ddot{\theta}_S$ at each of the two frequencies can be found by

$$A(\Omega) = A_n(\Omega) = |\ddot{\theta}(s)|_{s=j\Omega}, \quad (111)$$

where A_n is the zero-peak amplitude of the disturbance corresponding to the frequency chosen. Therefore, the amplitude of the fundamental frequency is

$$A_1 = \left| \frac{(-\frac{I_R}{I_S} j\Omega) (3-2.6)}{(I_R - K K_M \frac{I_R}{I_S} k_{\theta_S}^{\cdot\cdot})j\Omega + (K K_M k_{\theta_R}^{\cdot} + K_M)} \right| \text{ rad/s}^2. \quad (112)$$

Similarly, the amplitude of the second harmonic is

$$A_2 = \left| \frac{\left(-\frac{I_R}{I_S} 2j\Omega\right) (488.2)}{\left(I_R - K K_M \frac{I_R}{I_S} k_{\theta_S}''\right) 2j\Omega + \left(K K_M k_{\theta_R}' + K_M\right)} \right| \text{ rad/s}^2. \quad (113)$$

where Ω is the nominal rotor speed. These expressions can be utilized to compute predicted vibration levels for different values of the variable parameters K , k_{θ_R}' , and k_{θ_S}'' . In addition, these expressions can be utilized to predict vibration levels for different values of the motor gain, K_M .

Different values for the motor gain, K_M , may be implemented by changing the motor without adding any control components. This case may be examined by setting $K = 1$, and $k_{\theta_S}'' = k_{\theta_R}' = 0$ in Eqs. 112 and 113. With no feedback and variable K_M , the nominal speed of the rotor will not be constant. The applicable relationship is Eq. 105 with $K = 1$ and $k_{\theta_R}' = 0$,

$$\left. \dot{\theta}_R \right|_{ss} = 94.25 - \frac{203.4}{K_M} \text{ rad/s}. \quad (114)$$

Therefore, the frequency term, Ω , in Eqs. 112 and 113 is not constant. For this case, Eqs. 112 and 113 reduce to

$$A_1 = \left| \frac{\left(-\frac{I_R}{I_S} j\Omega\right) 352.6}{I_R j\Omega + K_M} \right| \text{ rad/s}^2, \text{ and} \quad (115)$$

$$A_2 = \left| \frac{\left(-\frac{I_R}{I_S} 2j\Omega\right) 488.2}{I_R 2j\Omega + K_M} \right| \text{ rad/s}^2. \quad (116)$$

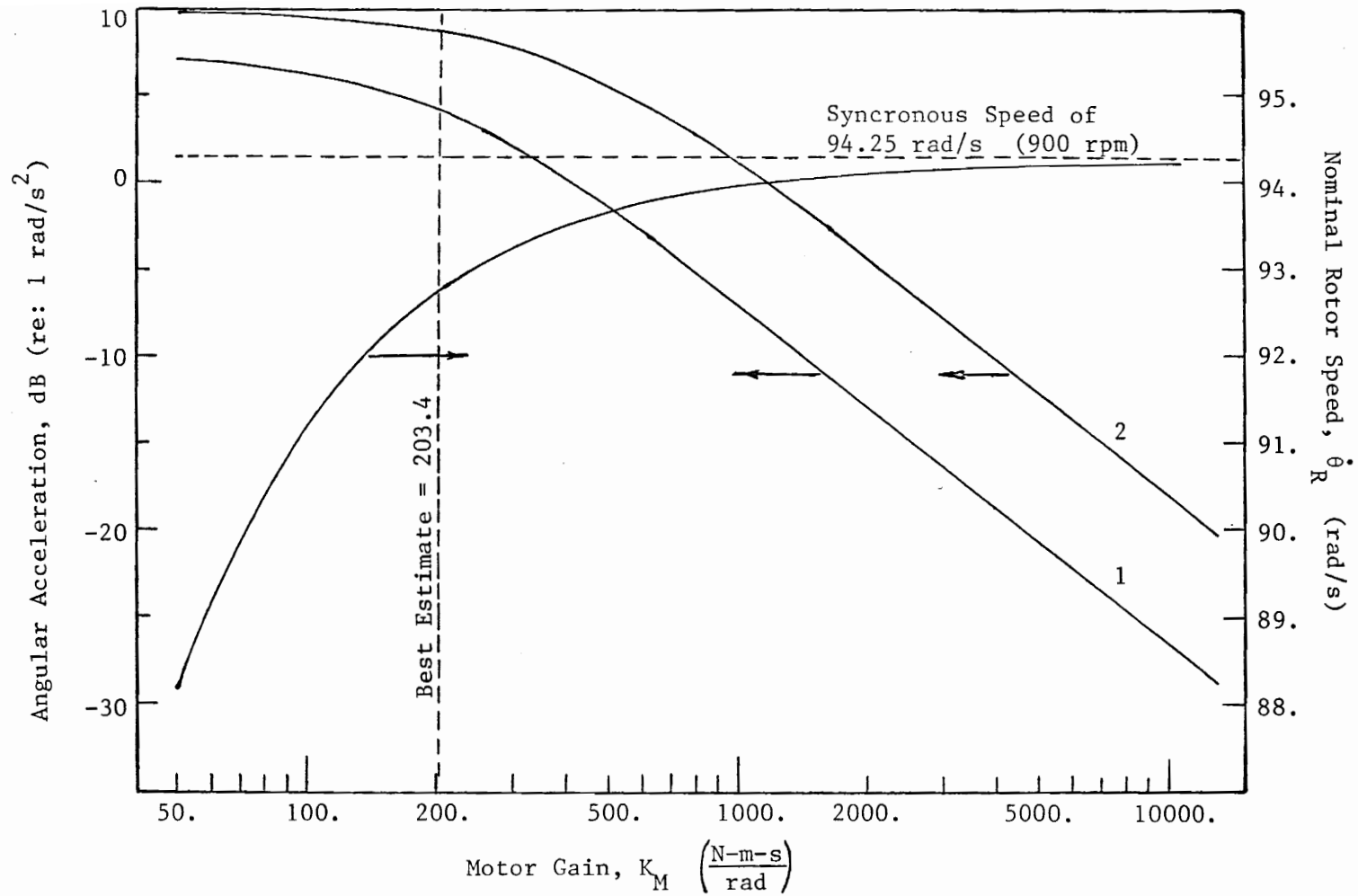
Table 8 shows the values for rotor speed and the amplitudes of the first and second harmonics of angular acceleration for different values of motor gain K_M . The value of 203.4 N-m-s/rad is the best-estimate value for the presently utilized motor. These data are also presented graphically in Fig. 27. As can be seen, an increase in the motor gain results in a decrease in roll acceleration levels and an increase in the rotor speed towards the synchronous speed of 94.25 rad/s. For example, a 10-fold increase in K_M results in a 17 dB reduction of the first harmonic, a 13 dB reduction in the second harmonic, and a 1.4% increase in the rotor speed.

Going back to Eqs. 112 and 113, the effect of K , $k_{\theta_R}^*$, and $k_{\theta_S}^{**}$ can be calculated. The data are plotted in Fig. 28. There are two independent variables in these equations. They are K and $k_{\theta_S}^{**}$. Choosing a value for K gives the value for $k_{\theta_R}^*$ (from Eq. 107) in order to keep the rotor speed at its "target" speed of 92.76 rad/s.

As can be seen from Fig. 28, reductions in roll vibration levels are obtained with increasing values of either the controller gain, K , or the roll acceleration feedback coefficient, $k_{\theta_S}^{**}$. These reductions are significant. For example, with a controller gain of 10 and a roll acceleration feedback coefficient of -10, the first harmonic amplitude has been attenuated 39.5 dB. The reduction of the second harmonic

Table 8. Effect of Motor Gain on Roll Vibration Levels

Motor Gain, K_M		Acceleration Levels (re: 1 rad/s ²)		Rotor Speed
N-m-s/rad	(ft-lbt-sec/rad)	Harmonic 1	Harmonic 2	rad/s
50.0	(36.9)	7.0	9.9	88.2
100.0	(73.8)	6.3	9.6	91.2
150.0	(110.6)	5.3	9.3	92.2
203.4	(150.0)	4.2	8.9	92.8
300.0	(221.3)	2.1	7.9	93.2
600.0	(442.6)	-2.8	4.7	93.7
1000.0	(737.6)	-6.9	1.2	94.0
2000.0	(1475.2)	-13.0	-4.3	94.1
4000.0	(2950.4)	-18.8	-10.2	94.2
10000.0	(7376.0)	-26.7	-18.1	94.2



$$1 \frac{N-m-s}{rad} = 0.7376 \frac{ft-lbf-s}{rad}$$

Figure 27. Effect of Motor Gain, K_M , on the Motor-Compressor System

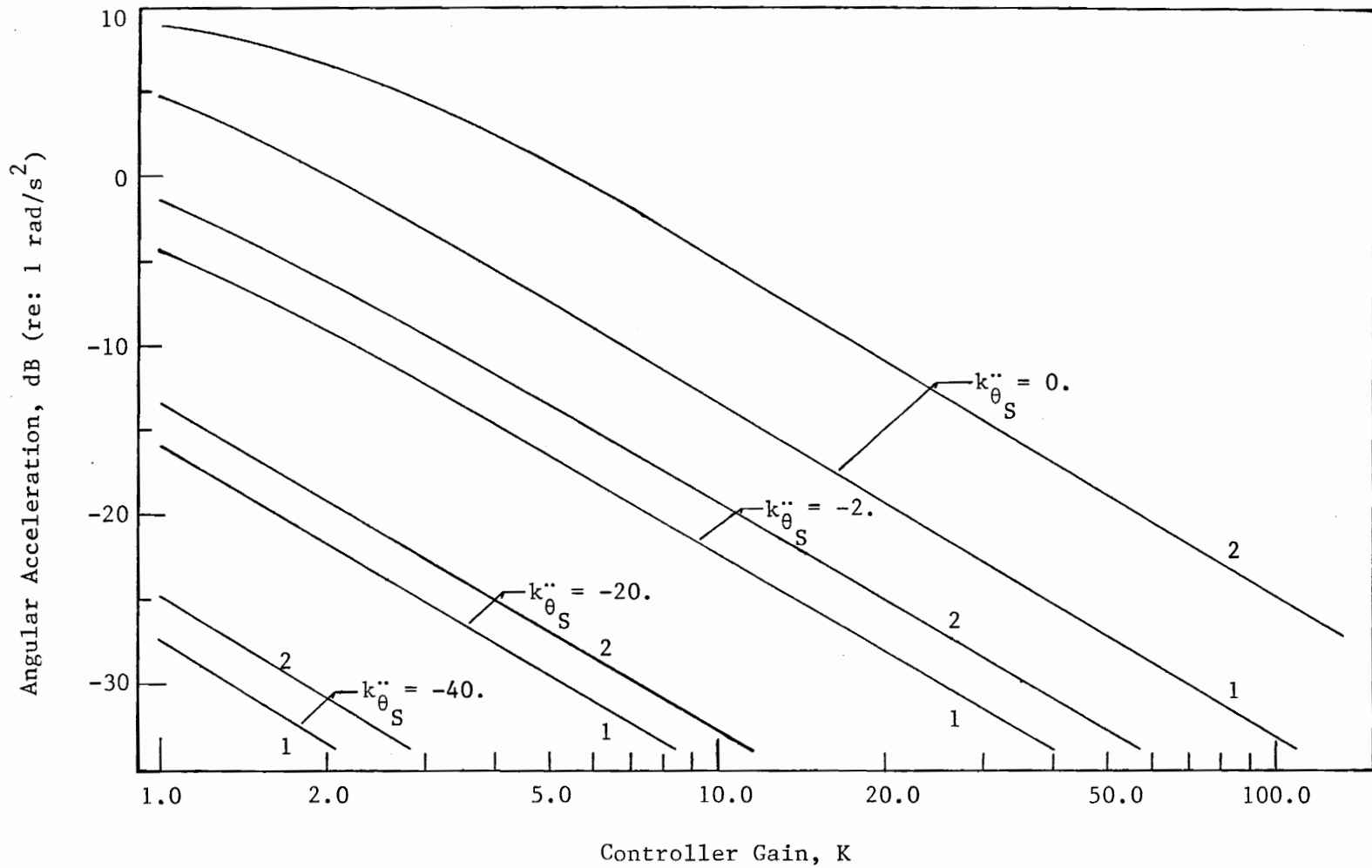


Figure 28. Effect of Varying the Controller Gain and the Feedback Gain

amplitude is 41.5 dB.

The implementation of this controller may be straightforward depending on the availability of certain components. The measurement of the two variables for the feedback loop, $\dot{\theta}_R$ and $\ddot{\theta}_S$ should be easily accomplished. However, obtaining a variable frequency controller with sufficient speed of response may be a limiting factor on this design. Initial contacts with vendors indicate that a controller suitable for this task is a state-of-the-art design.

As previously indicated, increasing the motor gain, K_M , will also reduce the roll acceleration levels of the shell. There are indications that this gain can be easily be increased by a factor of five or more (6).

8. CONCLUSIONS

At this point an overview of the entire study is in order. First, a motion analysis of the test compressor was carried out. Through this analysis the contribution of roll vibration was accurately determined. Next, a computer simulation of the test motor-compressor system was developed for use in a parametric study. Based on this parametric study, design curves were developed for the design of compressors with reduced roll vibration levels. Lastly, the system was analyzed and simplified using control theory. Theoretical controllers, some employing feedback, were developed, and their theoretical characteristics were determined.

Using data from three accelerometer positions on a machine a thorough motion analysis as developed in this study can be carried out. All three of the considered modes, roll, pitch, and z-direction translation, were found to contribute significantly to the observed vibration levels in the test compressor. The information gained through this analysis can be used for several purposes. A few purposes might be the location of mounts for minimum vibration transmission, and the location of vibration sensitive equipment such as gages, on the machine.

The development of the simulation program PABEWE used in the parametric study demonstrated that under most conditions, the standard assumptions used in dynamic analysis (such as constant speed shaft and stationary shell) introduce little error in the predicted forces. The parametric study conducted yielded interesting results. Varying the moment of inertia of the shell had the expected effect on the roll

vibration of the shell. The vibration was inversely proportional to the shell moment of inertia. Decreasing the moment of inertia of the rotor decreased the roll vibration of the shell. Varying piston mass provided the unexpected result of a shell roll vibration minima at a piston mass multiplier of about 2. Finally, if the piston pressure forces are equalized, then essentially no roll vibration-producing phenomena occur on a once-per-revolution basis, essentially eliminating roll vibration levels at the odd numbered harmonics.

The portion of the study devoted to the control of roll vibration provided analytical methods of controlling roll vibration. It was analytically demonstrated that a control system consisting of sensors for shell roll acceleration and rotor speed, a frequency or voltage controller, and some electronics, could be implemented to reduce shell roll vibration levels. Additionally, this section analytically demonstrated that a motor with a higher gain (torque-per-slip ratio) would result in lower shell roll vibration levels.

9. RECOMMENDATIONS

The recommendations offered are various and therefore will be listed numerically.

1. It is recommended that a motor be designed and built with a higher motor gain, i.e., torque-per-slip ratio, than that of the present motor. There are indications that this gain can be easily increased by a factor of five or more (6), for a considerable attenuation of roll vibration.
2. Considering that z-direction translation and pitch contribute significantly to observed compressor vibration levels, it is recommended that the technology herein developed be applied to a "perfectly balanced" compressor.
3. It is recommended that the design curves be used as a guide for future compressor designs. While there will be conflicting design requirements, these curves will provide an awareness of the roll vibration implications of various design parameters, e.g., flywheels increase roll vibration levels.
4. It is recommended that the motion analysis be used for the placement of mounts and other components which are sensitive to vibration. Such an analysis would eliminate the need for taking data at each mount, etc., to develop a vibration profile of the machine (at low frequencies).

5. It is recommended that a dynamic motor model be developed for use in PABEWE for a more accurate simulation. Additionally, a simple modification to PABEWE would provide a ten to one increase in the accuracy of the period estimation facility within PABEWE. This would involve only an interpolation scheme.

All these recommendations are mutually independent, allowing the implementation of any of them.

CITED REFERENCES

1. Gatecliff, G. W., "Analytical Analysis of the Forced Vibration of the Sprung Mass of a Reciprocating Hermetic Compressor, Including Comparison with Experiment," Proceedings of the 1974 Purdue Compressor Technology Conference, West Lafayette, Indiana, 1974.
2. Ishii, N., K. Imaichi, N. Kagoroku, and K. Imasu, "Vibration of a Small Reciprocating Compressor," ASME paper, 75-DET-44, 1975.
3. Beer, F. P., and E. R. Johnston, Jr., Vector Mechanics for Engineers: Statics and Dynamics, McGraw-Hill, New York, 1972.
4. Mabie, H. H., and F. W. Ocvirk, Dynamics of Machinery, John Wiley and Sons, New York, Third Edition, 1975.
5. Atherton, D. P., Nonlinear Control Engineering, Van Nostrand Reinhold Company, New York, 1975.
6. Personal communication with Mr. W. Brozek, General Dynamics Co., Newark, N.J., 16 Aug., 1977.

APPENDIX A

CSMP Simulation Code for the
Motor-Compressor System:

PABEWE

```

*****
*
* PABEWE-SIMPLE9, WRITTEN 7/25/77 BY JOHN H. HEROLD.
* THIS PROGRAM SIMULATES A TWO CYLINDER, MOTORIZED,
* UNMOUNTED, INLINE, RECIPROCATING AIR COMPRESSOR.
*
*****

```

```

FORMAT STATEMENT 100 OMITTED FROM THIS RECORD DUE TO LENGTH.
/ 101 FORMAT (4X,I2,T13,F5.1,5X,F5.3)
FORMAT STATEMENT 102 OMITTED FROM THIS RECORD DUE TO LENGTH.
FORMAT STATEMENT 103 OMITTED FROM THIS RECORD DUE TO LENGTH.
/ 104 FORMAT (2X,I3,2X,F6.5)

```

INITIAL

```
* _____
```

```

STORAGE REVHST(20),PERIOD(20),ERR(20),LEVEL(10),PHASE(10)
TABLE ICA(1-10)=10*0.0, ICB(1-10)=10*0.0
FIXED IREV,JREV,AA,BB,FACTOR,I,NHRMNC,CC
METHOD RECT

```

```
* _____
```

```
* INPUT CRANK PIN RADIUS IN MM AND CON. ROD LENGTH IN MM.
PARAMETER RADIUS=63.5, LENGTH=292.1
```

```
* INPUT WEIGHT OF PISTONS AND CON. ROD ENDS IN NEWTONS.
PARAMETER WAIT1=104.7, WAIT2=76.5
```

```
* INPUT THE POLAR MASS MOMENT OF INERTIA OF THE ROTOR
* AND SHELL, IN N-M SQ.
PARAMETER IRM2N=20.7, ISM2N=1488.
```

```
* INPUT INITIAL ROTOR AND SHELL SPEEDS
* IN REVOLUTIONS PER SECOND. (COUNTER CLOCKWISE)
INCON INRRPS=15., INSRPS=0.
```

* INPUT INITIAL ROTOR AND SHELL ANGLES
 * IN DEGREES FROM VERTICAL. (COUNTER CLOCKWISE)
 INCON INRANG=0., INSANG=0.

* THE NEXT PARAMETER STATEMENT LOADS CONTROL DATA.
 PARAMETER PRDERR=1., NHRMNC=10

* INPUT CONSTANTS
 CONSTANT PI=3.141592654 , GRVCON=9.8066
 PI2 =2.*PI

* THIS MODEL INCLUDES NO MOUNTS.
 TMOUNT=0.0

* THE FOLLOWING CARDS LOAD THE POINTS OF THE
 * MOTOR TORQUE CURVE (RPM , N-M).

FUNCTION TCURVE=(0.,0.),(6.,239.),(11.,361.),(20.,485.),...
 (34.,616.),(40.,744.),(70.,949.),(108.,1009.),...
 (180.,949.),(300.,746.),(500.,610.),(900.,542.)

* THE FOLLOWING CARDS LOAD THE POINTS OF THE FIRST STAGE
 * PISTON PRESSURE FORCES (BETA/10 , N)

FUNCTION PFCRV1= (0.,21472.),(1.,17704.),(2.,14150.),...
 (3.,11516.),(4.,7860.),(5.,5445.),(6.,3599.),(7.,2691.),...
 (8.,2349.),(9.,2282.),(10.,2273.),(11.,2282.),(12.,2531.),...
 (13.,2682.),(14.,2736.),(15.,2971.),(16.,3016.),...
 (17.,3176.),(18.,3145.),(19.,3252.),(20.,3416.),...
 (21.,3768.),(22.,3941.),(23.,4524.),(24.,4964.),...
 (25.,5663.),(26.,6588.),(27.,8287.),(28.,10409.),...
 (29.,13193.),(30.,17188.),(31.,20715.),(32.,22450.),...
 (33.,22810.),(34.,22784.),(35.,22428.),(36.,21472.)

* THE FOLLOWING CARDS LOAD THE POINTS OF THE SECOND STAGE
 * PISTON PRESSURE FORCES (BETA/10 , N)

FUNCTION PFCRV2= (0.,6499.),(1.,6481.),(2.,6770.),...
 (3.,7046.),(4.,7375.),(5.,7949.),(6.,8750.),(7.,9635.),...
 (8.,10849.),(9.,12446.),(10.,15204.),(11.,18847.),...
 (12.,23762.),(13.,29545.),(14.,33873.),(15.,34536.),...
 (16.,35070.),(17.,33931.),(18.,32783.),(19.,31516.),...
 (20.,26213.),(21.,21596.),(22.,16632.),(23.,13002.),...
 (24.,10284.),(25.,8243.),(26.,7437.),(27.,6881.),...
 (28.,6392.),(29.,6219.),(30.,6219.),(31.,6308.),...
 (32.,6534.),(33.,6592.),(34.,6663.),(35.,6637.),(36.,6499.)

* CONVERT INITIAL ROTOR AND SHELL SPEEDS
 * TO RADIANS PER SECOND.

INRSPD =INRRPS*PI2

INSSPD =INSRPS*PI2

* CONVERT INITIAL ROTOR AND SHELL ANGLES TO RADIANS.

INRA =INRANG*PI/180.

INSA =INSANG*PI/180.

* CONVERT CRANK RADIUS AND CONNECTING ROD LENGTH TO METERS.

R =RADIUS/1000.

L =LENGTH/1000.

* CONVERT INERTIAS TO KG-M SQ.

IR =IRM2N/GRVCON

IS =ISM2N/GRVCON

* CONVERT THE WEIGHT OF THE PISTONS TO KILOGRAMS.

M1 =WAIT1/GRVCON

M2 =WAIT2/GRVCON

DYNAMIC

* _____

* THE NEXT FOUR STATEMENTS ARE THE FOUR BASIC INTEGRALS.

AR DOT =INTGRL (INRSPD,ARDDOT)

AS DOT =INTGRL (INSSPD,ASDDOT)

AR =INTGRL (INRA, AR DOT)

AS =INTGRL (INSA, AS DOT)

* _____

* NOW THE DIFFERENCES IN ANGULAR POSITIONS , 'BCONT',

* AND ANGULAR VELOCITIES , 'OMEGA', BETWEEN THE

* SHELL AND THE ROTOR, ARE CALCULATED.

BCONT=AR-AS

OMEGA=AR DOT-AS DOT

* _____

* THE FOLLOWING PROCEDURE HOLDS THE OPERATIONAL BETA
 * TO LESS THAN 2 PI.
 * TO LESS THAN 2 PI.

```
PROCEDURE  B,JREV=BETH(BCONT)
  JREV=0
  B=BCONT
  10 IF (B .LE. PI2 ) GO TO 11
  JREV=JREV+1
  B=B-PI2
  GO TO 10
  11 IF (B .GE. 0.0) GO TO 12
  B=B+PI2
  GO TO 11
  12 CONTINUE
ENDPRO
```

* _____

* THE FOLLOWING STATEMENTS DETERMINE THE MOTOR TORQUE AS A
 * FUNCTION OF 'OMEGA'. (TORQUE IS 'TSLIP')

```
SLIP      =900.-OMEGA*60./PI2
ABSLIP    =ABS(SLIP)
TSLIP     =AFGEN (TCURVE,ABSLIP)
```

* _____

* THE FOLLOWING PROCEDURE DETERMINES
 * THE SIGN OF THE MOTOR TORQUE.

```
PROCEDURE  TMR=BANNER(TSLIP, SLIP)
  IF (SLIP .GE. 0.) GO TO 20
  TMR=-TSLIP
  GO TO 21
  20 TMR=TSLIP
  21 CONTINUE
ENDPRO
```

* _____

* THE FOLLOWING CARDS INTERPOLATE THE PRESSURE FORCE CURVES.
 * A QUADRATIC INTERPOLATION ALOGRITHM WAS USED.

```
BDEG      =B*180./PI
BDEG10    =BDEG/10.
PF1=NLFGEN(PFCRV1,BDEG10)
PF2=NLFGEN(PFCRV2,BDEG10)
```

* _____

* THE FOLLOWING STATEMENTS ULTIMATELY DETERMINE
* ARDDOT AND ASDDOT EXPLICITELY.

```

TMS      =-TMR
SINB     =SIN(B)
COSB     =COS(B)
SIN2B    =SIN(2.*B)
COS2B    =COS(2.*B)
FI1      =ARSIN(R*SINB/L)
FI2      =-FI1
SINFI1   =SIN(FI1)
COSFI1   =COS(FI1)
SINFI2   =-SINFI1
COSFI2   =COSFI1
SINBF1   =SIN(B+FI1)
SINBF2   =SIN(B+FI2)
RM1      =R*COSB+L*COSFI1
RM2      =RM1-2.*R*COSB
RMDOT1   =-(R*OMEGA*SINB+R**2*OMEGA*SIN2B/(2.*L))
RMDOT2   =RMDOT1+2.*R*OMEGA*SINB
E        ={M1*RM1*RMDOT1+M2*RM2*RMDOT2}*2.*ASDOT
ISS      =IS+M1*RM1**2+M2*RM2**2
C1       =RM1*SINFI1/COSFI1
C2       =RM2*SINFI2/COSFI2
C3       =R*SINB
C4       =R*OMEGA**2*COSB
C5       =R**2*SIN2B/(2.*L)
C6       ={R*OMEGA}**2*COS2B/L
C7       =RM1*ASDOT**2
C8       =RM2*ASDOT**2
C9       =TMS+TMOUNT-E
C10      =-R*SINBF1/COSFI1
C11      =R*SINBF2/COSFI2
C12      =C4+C6+C7
C13      =-C4+C6+C8
C14      =C3+C5
C15      =-C3+C5
C16      =C1*M1*C14+C2*M2*C15
C17      =C10*M1*C14+C11*M2*C15
C18      =C9+C1*(M1*C12-PF1)+C2*(M2*C13-PF2)
C19      =TMR+C10*(M1*C12-PF1)+C11*(M2*C13-PF2)
C20      =C18*(IR-C17)+C19*C16
C21      =IR*ISS+C16*IR-C17*ISS
ASDDOT   =C20/C21
ARDDOT   =C19/(IR-C17)-C16*C17*C19/(C21*(IR-C17))-C17*C18/C21
* _____

```

* AS A CONTINUOUS CHECK, CALCULATE
* THE TOTAL SYSTEM ANGULAR MOMENTUM.

H= ASDOT*ISS + ARDOT*IR

* _____

* THE FOLLOWING PROCEDURE SETS HO = TO H INITIAL.

```
PROCEDURE HO=FUNCT(H,TIME)
  IF (TIME .EQ. 0.0) HO=H
ENDPRO
```

* _____

* THE FOLLOWING PROCEDURE PROVIDES THE CONTROL LOGIC
 * NEEDED TO TURN ON THE RTA WHEN THE COMPRESSOR PERIOD
 * CHANGE IS WITHIN A CERTAIN PERCENTAGE CHANGE SPECIFIED
 * AS 'PRDERR'. IT ALSO TERMINATES THE SIMULATION WHEN
 * ONE COMPLETE CYCLE HAS BEEN FED TO THE RTA.

```
PROCEDURE FACTOR,T,P,IREV,TRMTIM=TRIGER(BCONT,...
  PRDERR,TIME,PI2,JREV)
  IF (TIME .EQ. 0.) FACTOR=0
  IF (TIME .EQ. 0.) IREV=0
  AA=0
  BB=0
  IF (JREV .EQ. IREV) GO TO 31
  AA=1
  IREV=JREV
  REVHST(IREV)=TIME
  IF (IREV .EQ. 1) GO TO 30
  PERIOD(IREV)=REVHST(IREV)-REVHST(IREV-1)
  EROR=ABS((PERIOD(IREV)-PERIOD(IREV-1))/PERIOD(IREV-1))
  ERR(IREV)=EROR
  IF ((EROR*100.) .GT. PRDERR) GO TO 31
  BB=1
  GO TO 31
30 PERIOD(1)=REVHST(1)
31 CONTINUE
  IF (FACTOR .EQ. 1) GO TO 32
  IF (BB .EQ. 1) GO TO 33
  GO TO 34
32 IF (AA .NE. 1) GO TO 34
  TRMTIM=TIME
  CALL FINISH
33 FACTOR=1
34 CONTINUE
  IF (IREV .EQ. 0) GO TO 35
  T=TIME-REVHST(IREV)
  P=PERIOD(IREV)
  GO TO 36
35 T=TIME
  P=1.
36 CONTINUE
ENDPRO
```

* _____


```
* THE FOLLOWING PROCEDURE PREPARES THE MODULATED
* FUNCTIONS FOR INPUT TO THE RTA INTEGRATORS.
PROCEDURE AAAA,BBBB=MDULAT(ASDDOT,T,P,PI2,NHRMNC,FACTOR)
  DO 40 I=1,NHRMNC
    AAAA(I)=FACTOR*ASDDOT*COS(I*PI2*T/P)
    40 BBBB(I)=FACTOR*ASDDOT*SIN(I*PI2*T/P)
ENDPRO
```

```
* _____
```

```
* THE FOLLOWING STATEMENTS ESTABLISH THE INTEGRATOR
* ARRAYS FOR THE RTA SIMULATION (REAL TIME ANALYZER).
COEFA=INTGRL (ICA,AAAA,10)
COEFB=INTGRL (ICB,BBBB,10)
```

```
* _____
```

```
* THE FOLLOWING STATEMENTS PREPARE SOME OUTPUT OCCASIONALLY
* OF INTEREST. SELDOMLY USED STATEMENTS MAY BE COMMENTED OUT
* THROUGH THE USE OF AN '*' IN COLUMN 1.
*PCSPED=(C/(PI2*15.))*100.
*PCFULD=INSTHP/60.)*100.
*INSTHP=TMR*(OMEGA*60./PI2)/5250.
*INSTKW=INSTHP*0.7456
*ASDEG=AS*180./PI
FREQ=1./P
*RPM=60.*FREQ
```

TERMINAL

*

* THE FOLLOWING STATEMENTS WORK UP THE
 * LEVEL AT EACH HARMONIC OF ROTATIONAL FREQUENCY
 * (IN DB. RE: 1.RAD/SEC.SQ.)
 DO 50 I=1,NHRMNC
 COEFC=1./(P/2.)*SQRT(COEFA(I)**2+COEFB(I)**2)
 LEVEL(I)=20.*ALOG10(COEFC)
 PHASE(I)=ATAN(COEFB(I)/COEFA(I))
 IF (COEFA(I) .LT. 0.) PHASE(I)=PHASE(I)+PI
 IF (COEFA(I) .LT. 0.) GO TO 50
 IF (COEFB(I) .LT. 0.) PHASE(I)=PHASE(I)+PI2
 50 CONTINUE

*

* THE FOLLOWING CARDS PREPARE THE OUTPUT FORMAT.
 * (NORMALLY, SEVERAL STATEMENTS SPECIFYING THE VARIABLES TO
 * BE OUTPUT AND THEIR APPROPRIATE FORMAT, I.E. GRAPH,
 * LIST, ETC., WOULD APPEAR HERE.)
 WRITE (6,100) FREQ
 DO 60 I=1,NHRMNC
 60 WRITE (6,101) I,LEVEL(I),PHASE(I)
 HERROR=ABS(HO-H)/HO*100.
 IF (HERROR .GE. 0.1) GO TO 61
 WRITE (6,102) HERROR
 GO TO 62
 61 WRITE (6,103) HERROR
 62 CONTINUE

* THE FOLLOWING STATEMENT SPECIFIES THE DURATION OF THE
 * SIMULATION, 'FINTIM' (IN SECONDS), AND THE INTERVAL OF
 * TIME BETWEEN OUTPUTS, 'OUTDEL' (IN SECONDS).
 TIMER FINTIM=0.50, DELT=.0005, OUTDEL=0.001

* THIS CONCLUDES THE CURRENT VERSION OF PABEWE.

*

END
 STOP

THE FOLLOWING DATA ARE THE LEVELS OF THE FIRST TEN HARMONICS OF THE ROTATIONAL FREQUENCY OF 14.8 HZ.

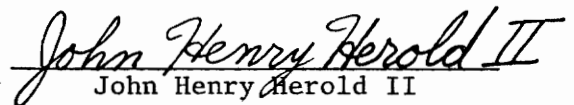
HARMONIC	LEVEL, DB. (RE: 1 RAD./SEC.SQ.)	PHASE
1	4.3	0.957
2	8.9	3.789
3	0.2	1.153
4	0.4	3.492
5	-22.2	1.815
6	-15.0	0.455
7	-18.2	3.616
8	-20.0	6.156
9	-25.1	3.203
10	-26.6	4.455

THE DYNAMIC ANALYSIS IS PROBABLY CORRECT, SINCE THE TOTAL SYSTEM ANGULAR MOMENTUM VARIED BY ONLY 0.0029 %.

VITA

The author, John Henry Herold II, was born October 10, 1953, in Baltimore, Maryland. In the Fall of 1971 he entered Virginia Polytechnic Institute and State University, where he majored in Mechanical Engineering. He also participated in the Co-operative Education program, receiving employment as a student-trainee at the David Taylor Naval Ship Research and Development Center, DTNSRDC, at Annapolis, Maryland.

In June 1976 he was graduated and was awarded the Bachelor of Science Degree in Mechanical Engineering. Upon graduating he accepted a position as a Mechanical Engineer at DTNSRDC, Annapolis, Maryland. He requested and received a one-year leave of absence from DTNSRDC to pursue graduate studies. He received a graduate research assistantship and began his graduate studies at VPI&SU in the Fall of 1976.


John Henry Herold II

ROLL VIBRATION OF A RECIPROCATING AIR COMPRESSOR

by

John Henry Herold II

(ABSTRACT)

The rigid-body rotational vibration of a resiliently mounted air compressor about an axis parallel to the axis of the rotor is investigated.

An analysis of the motion of the compressor base is conducted using empirical acceleration data. The effect on roll vibration of changing various compressor design parameters is studied using a computer simulation program, PABEWE. This digital simulation incorporating slider-crank linkage analysis employs the strict equations of motion.

Control theory is used to control the roll vibration. The control theory is applied to simplified equations of motion and incorporates various feedbacks. Recommendations are offered for the reduction of roll vibration levels.